Dawn: A journey in space and time

C.T. Russell[a,*], A. Coradini[b], U. Christensen[c], M.C. De Sanctis[d], W.C. Feldman[e], R. Jaumann[f], H.U. Keller[c], A.S. Konopliv[g], T.B. McCord[h], L.A. McFadden[i], H.Y. McSween[j], S. Mottola[f], G. Neukum[k], C.M. Pieters[l], T.H. Prettyman[e], C.A. Raymond[g], D.E. Smith[m], M.V. Sykes[n], B.G. Williams[g], J. Wise[o], M.T. Zuber[p]

[a]IGPP& ESS, UCLA, 3845 Slichter Hall, MS 156704, Los Angeles, CA 90095-1567, USA
[b]IFSI, Via del fosso del Cavaliere, Rome 00133, Italy
[c]MPAe, Katlenburg-Lindau, Germany
[d]IAFS, Via del fosso del Cavaliere, Rome 00133, Italy
[e]LANL, MS D466, NIS-1, Los Alamos, NM 87545, USA
[f]DLR Rutherfordstr 2, Berlin D-12489, Germany
[g]JPL, 4800 Oak Grove Dr., Pasadena, CA 91109, USA
[h]University of Hawaii, 2525 Correa Rd., Honolulu, HI 96822, USA
[i]University of Maryland, College Park, MD 20742, USA
[j]University of Tennessee, Knoxville, TN 37996-1410, USA
[k]Freie Universitat, Berlin, Malteser Str.74-100, Berlin 12249, Germany
[l]Brown University, Providence, RI 02912, USA
[m]GSFC, MC 920, Greenbelt, MD 20771, USA
[n]U of Arizona, Tucson, AZ 85721, USA
[o]New Roads School, Santa Monica, CA 90404, USA
[p]MIT, Cambridge, MA 02139, USA

Abstract

By successively orbiting both 4 Vesta and 1 Ceres the Dawn mission directly addresses the long-standing goals of understanding the origin and evolution of the solar system. Ceres and Vesta are two complementary terrestrial protoplanets (one apparently "wet" and the other "dry"), whose accretion was probably terminated by the formation of Jupiter. They provide a bridge in our understanding between the rocky bodies of the inner solar system and the icy bodies of the outer solar system. Ceres appears to be undifferentiated while Vesta has experienced significant heating and likely differentiation. Both formed very early in the history of the solar system and while suffering many impacts have remained intact, thereby retaining a record of events and processes from the time of planet formation. Detailed study of the geophysics and geochemistry of these two bodies provides critical benchmarks for early solar system conditions and processes that shaped its subsequent evolution. Dawn provides the missing context for both primitive and evolved meteoritic data, thus playing a central role in understanding terrestrial planet formation and the evolution of the asteroid belt. Dawn is to be launched in May 2006 arriving at Vesta in 2010 and Ceres in 2014, stopping at each to make 11 months of orbital measurements. The spacecraft uses solar electric propulsion, both in cruise and in orbit, to make most efficient use of its xenon propellant. The spacecraft carries a framing camera, visible and infrared mapping spectrometer, gamma ray/neutron spectrometer, magnetometer, and radio science.

1. Introduction

The Dawn mission investigates two of the first bodies formed in the solar system. 1 Ceres and 4 Vesta are complementary protoplanets that have remained intact since their formation. Ceres apparently incorporated water ice during accretion, slowing its thermal evolution while Vesta, smaller and closer to the Sun, apparently melted and differentiated. Dawn's goal is to orbit both asteroids to obtain measurements that provide an understanding of the conditions and processes acting at the solar system's earliest epoch. To do this Dawn investigates their internal structure,

* Corresponding author. Tel.: +1-310-825-3188; fax: +1-310-206-3051.

E-mail address: ctrussell@igpp.ucla.edu (C.T. Russell).

density and homogeneity by measuring their mass, shape, volume and spin state with radiometric tracking, and imagery. It records their remanent magnetization, and elemental and mineral composition to infer their thermal history and evolution. It provides context for meteorites that are believed to have come from Vesta. Dawn provides images of the surfaces of these two objects to determine their bombardment, tectonic and possibly volcanic history; it uses gravity, spin state and magnetic data place constraints on the size of any metallic core, and it employs IR, gamma-ray and neutron spectrometry to search for water-bearing minerals.

Dawn focuses on Ceres and Vesta, not simply because they are the two largest rocky planets that remain unexplored but because they should provide important clues to the processes taking place in the earliest phase of solar system formation. In addition, they form a bridge in our understanding, from the rocky bodies of the inner solar system to the icy bodies of the outer solar system. Radioisotope chronology from the howardite, eucrite, and diogenite (HED) meteorites, believed to be from Vesta, suggests it differentiated in perhaps only 3 million years (Yin et al., 2002; Kleine et al., 2002). Similar evidence indicates that Mars continued to differentiate for close to 15 million and Earth for 30 million years. The early cessation of accretion in the asteroid belt was presumably due to the formation of Jupiter whose gravitational forcing countered the accretionary process, and today is causing the disruption of the bodies that did accrete. Although we do not have similar meteorite evidence directly linked to Ceres, it too is expected to have formed in the first approximately 10 million years. In addition the asteroid belt may have been scoured by comets, scattered by the formation of the remaining gas giants (Gil-Hutton and Brunini, 1999). Today only some of the largest asteroids remain relatively undisrupted. The most massive of these (Hilton, 1999) are Ceres and Vesta, two most complementary minor planets. The former has a very primitive surface, water-bearing minerals, and possibly a very weak atmosphere and polar cap. The latter is a dry, differentiated body whose exterior has been resurfaced by basaltic lava flows possibly possessing an early magma ocean like the Moon. Vesta has experienced significant excavating events, most notably indicated by the huge crater near its southern pole (Thomas et al., 1997a). Cosmic ray exposure dating of HEDs indicates that impacts have produced meteoritic material at least five times in the last 50 million years (Eugster and Michel, 1995). These impacts may have occurred on vestoids, pieces of Vesta released at early times. The meteorites that have reached the Earth have been used to piece together a most probable scenario for Vesta's thermal evolution (e.g. Ghosh and McSween, 1998).

No meteorites have unmistakably come from Ceres. Possibly the excavating events or interplanetary dynamics that provided the HED meteorites did not occur at Ceres, but also, the reflectance spectrum of the surface of Ceres does not give unique signatures of its crustal rocks. Microwave studies suggest that Ceres is covered with a dry clay, in contrast to Vesta's basaltic dust layer that reflects its crustal composition (Webster and Johnston, 1989). To determine if we have Ceres-derived meteorites and to understand Ceres' origin, it is necessary to go there and obtain spectra inside fresh craters.

Meteorites provide an incomplete glimpse of their parent bodies. To understand the thermal evolution of Vesta and Ceres a knowledge of their interior structure is required, as is an understanding of their geological and geophysical record. It is important to determine the geologic context for the HED meteorites from Vesta, and search for similar data for Ceres. We are especially interested in contrasting dry, differentiated Vesta with its wet counterpart, Ceres, just a little further from the Sun. It appears that a rather short additional radial separation allowed Ceres to accrete wet and stay cool while early heat sources (^{26}Al?) in the accreting material melted Vesta. Most importantly, because they both lie near the ecliptic plane in near-circular orbits, it is possible to rendezvous with and study both using a single Discovery mission.

While there have been three previous asteroid flybys and one previous asteroid rendezvous, none of these missions have been at all comparable to Dawn. Galileo has flown by two small asteroids, the S-types, Gaspra and Ida, obtaining visible imagery. In 1997, NEAR flew by the C-class asteroid, 253 Mathilde, obtaining images and deriving its mass. In 2000, NEAR entered orbit about the 30-km long, S-type asteroid 433 Eros with a payload similar to that of Dawn but there the resemblance stops. Eros is a very homogeneous body, likely a fragment of a larger body. Vesta shows signs of a metallic core, as implied from studies of the HED meteorites, a Mars-like density and lunar-like basaltic flows, so Mars and lunar data comparisons may be more relevant than those with Eros. Further the action of water on the surface of Mars will be compared and contrasted with the possible effects of water on Ceres. In addition Voyager, Galileo, and Cassini provide contrasting data on the structure of water-rich small bodies in the outer solar system.

While our first closeup data from asteroids was obtained only slightly over a decade ago, remote sensing data have been obtained for over 200 years. In the late 18th century it was recognized that the planets were spaced in a regular manner according to a formula now called the Titius-Bode law. Baron von Zach, a German astronomer, believed that this law predicted a planet between Mars and Jupiter and initiated the first international science campaign to discover its location. However, an Italian observer, not part of the search team, Giuseppe Piazzi, found Ceres at the expected distance from the Sun on January 1, 1801. It was with some surprise that a second object Pallas, was discovered during the course of monitoring Ceres. Pallas' discovery was followed by 3 Juno. Later, on March 29, 1807 a member of Von Zach's team, the German astronomer, H. Olbers, discovered 4 Vesta. Owing to their small size and large distance even today we have little information on these two bodies. The Hubble Space Telescope enables us to resolve only
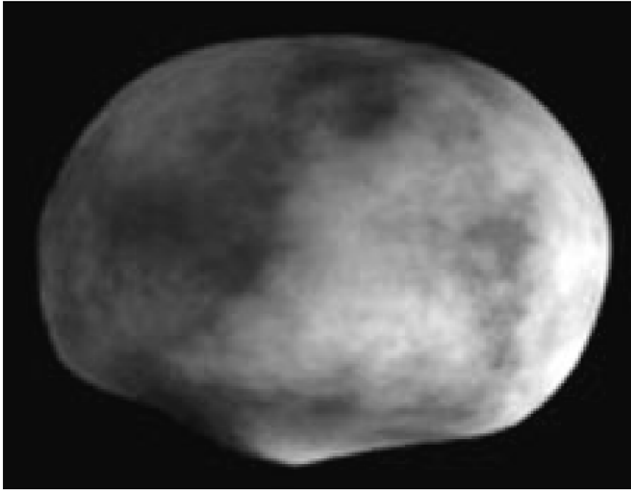
Fig. 1. Vesta shape model (Zellner and Thomas, 1997).

the very largest scale features on their surfaces as shown in Fig. 1, for Vesta. To determine the detailed elemental and mineral composition, the tectonic and thermal evolution, the internal structure, and the possible presence of magnetic fields and a metallic core we must travel to these bodies.

While the scientific community has long recommended missions to Vesta and/or Ceres, the Deep Space 1 mission's demonstration of the solar electric ion thrusters has only now enabled a mission to visit these bodies successively, orbiting each, and fitting within the Discovery cost envelope. Our science strategy and instruments are optimized for this mission as we build on extensive ground-based and HST-based studies of both objects and studies of their meteorite analogs.

2. Current understanding

4 Vesta and 1 Ceres are among the most massive asteroids. Both orbit the Sun and are large enough to have experienced many of the processes normally associated with planetary evolution. They could rightly be considered small planets but, because of their locations within the asteroid belt, they have been classified as asteroids. Unlike most other objects in the main belt, which are battered relics of larger bodies, Vesta and Ceres have somehow survived intact through 4.5 billion years of collisional history that must have seen the destruction of most of their neighbors. These protoplanets carry retrievable records of physical and chemical conditions and nebular and geologic processes during the early planet-forming epoch.

Planetesimals like Vesta and Ceres formed by the accretion of smaller objects over short time scales. Accretion in the main belt apparently was terminated before the formation of planetary objects larger than Ceres and Vesta, presumably due to Jupiter, whose gravitational forcing countered the accretionary process. As we discuss in more de-

tail below, Ceres has a much lower density than does Vesta (about 2100 kg/m^3 vs. nearly 4000 kg/m^3, respectively) and Ceres is inferred to be volatile rich, while Vesta is dry. Yet these very different objects were apparently formed relatively close together in the solar system. It is one of Dawn's main science objectives to determine how and why.

Before describing the mission we present below a brief summary of what we understand about each object beginning with the object we visit first, Vesta. For those desiring even more details on our current understanding, Keil (2002) has provided a recent comprehensive review of what is presently known about Vesta. McCord and Sotin (2003) have provided a recent comprehensive review of what is presently known about Ceres and its possible thermal evolution tracks. Several other recent publications also give useful summaries of the general knowledge of Ceres and discuss and improve on the knowledge of its principal characteristics (Parker et al., 2002; Britt et al., 2002).

2.1. 4 Vesta

Vesta has a triaxial ellipsoid shape with radii of 289, 280, and 229 ± 5 km, based on HST imagery (Thomas et al., 1997b). Its mean radius is thus 258 ± 12 km, equivalent to a volume of $7.19 ± 0.87 × 10^7$ km^3. Vesta's mass has been estimated at $1.38 ± 0.12 × 10^{-10}$ solar masses (Schubart and Matson, 1979), $1.5 ± 0.3 × 10^{-10}$ solar masses (Standish and Hellings, 1989), and $1.36 ± 0.05 × 10^{-10}$ solar masses (Michalak, 2000). The densities calculated from these values range from 3200 ± 5050 kg/m^3.

Vesta is a dry, differentiated body whose surface has been covered by pyroxene-bearing basaltic lavas with composition like HED meteorites (McCord et al., 1970). Absorption band parameters reveal mineralogical variations as the asteroid rotates. As seen in both Earth-based (Gaffey, 1997; Cochran and Vilas, 1998) and HST (Binzel et al., 1997) spectra, the surface of Vesta contains abundant pyroxenes— Mg-rich and Ca-poor pyroxenes in the eastern hemisphere, and Fe- and Ca-rich pyroxenes in the western hemisphere. These variations, inferred to reflect impact-excavated plutonic rocks in the east and lava flows in the west, have not been petrologically homogenized by regolith formations or spectrally obscured by space weathering. The lack of space weathering has been attributed by Hiroi et al. (1994) to a scarcity of olivine, which may be the principal mineral altered by this process (Yamada et al., 1999). However, the surface of the moon is weathered and it lacks olivine also. Whether the crust formed by serial magmatism or solidification of a magma ocean is unclear. Vesta has experienced significant impact events, one of which excavated a huge (460 km diameter) crater near its south pole (Thomas et al., 1997a). Spectral variations within this large crater (Thomas et al., 1997b) demonstrate compositional stratigraphy, probably reflecting a mantle and/or lower crust enriched in olivine relative to surficial flows.

The largest (100 meteorites) class of achondrites, the HED association, is commonly believed to have been derived from Vesta (Consolmagno and Drake, 1977). The spectral characteristics of Vesta conform to those of HEDs, an almost unique match (only one other basaltic asteroid, 1459 Magnya, has been identified in the main belt (Lazzaro et al., 2000), and it is not located in a position that should be easily sampled). With the discovery of small, impact-ejected "Vestoids" spanning the gap between Vesta's orbit (Binzel and Xu, 1993) and the $\frac{3}{1}$ mean motion and ν_6 secular resonances with Jupiter which serve as escape hatches (Wisdom, 1985), the hypothesis that Vesta is the HED parent body has become widely accepted. Vestoids exhibit spectra similar to those of eucrites and howardites (Burbine et al., 2001), although subtle spectral differences exist (Vilas et al., 2000). These might have been ejected during formation of the south pole crater, which excavated $\sim 1\%$ of Vesta. However, cosmic-ray exposure ages of HEDs form clusters, suggesting they were produced possibly from vestoids, during several impact events (Eugster and Michel, 1995; Welten et al., 1997).

The HED achondrites crystallized under dry, reducing conditions very early in solar system history. Members of this group define a unique oxygen isotope mass fractionation line displaced below the terrestrial line (Clayton and Mayeda, 1996) and exhibit distinctive pyroxene (iron/manganese) and plagioclase (potassium/calcium) compositions (Papike, 1998). Cumulate and noncumulate eucrites are iron-rich gabbros and basalts composed mostly of pigeonite and calcic plagioclase. Diogenites are cumulate orthopyroxenites, sometimes with minor olivine, and howardites are regolith breccias composed of fragments of eucrites and diogenites. Attempts to relate eucrites and diogenites require complex igneous models involving melting scenarios that generated diverse liquids which produced a variety of cumulate rocks (Stolper, 1977; Longhi and Pan, 1988; Grove and Bartels, 1992) or fractional crystallization of an extensive magma ocean (Righter and Drake, 1997; Ruzicka et al., 1997; Warren, 1997). Assuming serial magmatism, Wilson and Keil (1996) modeled the sizes and flow rates of conduits that carried magmas from source regions to Vesta's surface.

The widths of augite exsolution lamellae in one cumulate eucrite indicate slow cooling, equivalent to a burial depth of ~ 8 km (Miyamoto and Takeda, 1994). This measurement may be taken as a minimum thickness of Vesta's crust, in agreement with the largest (< 10 km) eucrite Vestoid (Binzel and Xu, 1993). Many eucrites have suffered brecciation, recrystallization, or impact melting. Although much thermal modification is due to impact processes, Yamaguchi et al. (1996, 1997) suggested that subjacent parts of the crust of Vesta were metamorphosed when they were buried by successive lava flows and cooled slowly from peak temperatures.

Radiometric ages indicate that HEDs crystallized at ~ 4.56 Ga (Nyquist et al., 1997; Tera et al., 1997; Lugmair

and Shukolyukov, 1998, and references therein) and support an early and limited duration of igneous activity for Vesta. The heat source for melting was probably rapid decay of short-lived ^{26}Al, since evidence for this now-extinct isotope has been found in eucrites (Srinivasan et al., 1999). Rapid melting is also supported by the former presence in eucrites of ^{60}Fe, another short-lived radionuclide (Carlson and Lugmair, 2000).

Metal segregation (and likely core formation) on Vesta is indicated by depletion of siderophile elements (Ni, Co, Mo, W, P) relative to non-siderophile elements in HEDs (Hewins and Newsom, 1988; Righter and Drake, 1996). By modeling siderophile element abundances, modest core sizes (percentages of the asteroid by mass) of 21.7% (Dreibus et al., 1997), 0–25% (Ruzicka et al., 1997), and 5–25% (Righter and Drake, 1997) have been estimated. Natural remanent magnetization in HEDs suggest that this core generated an ancient global magnetic field, with a surface field similar to that of the Earth (5–50 μT) (Morden, 1992; Collinson and Morden, 1994). Based on HED ^{182}W/^{182}Hf ratios, core formation is thought to have occurred within 3 Ma of the solar system's formation (Yin et al., 2002; Kleine et al., 2002). This recently derived age is consistent with ^{26}Al playing a significant role in the heating of asteroids. A thermal evolution model for Vesta, based on heating by ^{26}Al and constrained by HED chronology, geochemistry and phase relations, was developed by Ghosh and McSween (1998). This model suggests that the interior of Vesta remained hot for considerably longer than the ages of crustal HED meteorites.

2.2. 1 Ceres

With its greater heliocentric distance, lower albedo, more spherical shape and fewer spectral features, we know less about the composition of Ceres than we do about Vesta. Fig. 2 shows our best present images of Ceres. Its location is compared to that of the semi-major axis of Vesta and other asteroids in the main belt in Fig. 3.

Three different methods of measuring the size and shape of Ceres have been employed: occultation of a star by Ceres as seen from the Earth, direct imaging by the earth-orbital Hubble Space Telescope camera, and adaptive optics while imaging from groundbased telescopes. These results are summarized in Table 1.

The mass of Ceres has been determined repeatedly with ever improving results. (Michalak, 2000; Viateau and Rapaport, 1998; Standish, personal communication 2001; Hilton, 1999); McCord and Sotin (2003) have reviewed the various mass and shape determinations and arrived at a model mass of $4.740 \pm 0.026 \times 10^{-10}$ solar masses or 9.43×10^{20} kg with an estimated uncertainty of 0.05×10^{20} kg or about 0.5% relative uncertainty. They calculated a formal model radius value of 475.04 km or a diameter of 950.08 km, with an estimated uncertainty of order 10 km in radius, or about 2%. This gives a density for Ceres of 2100 kg/m^3.
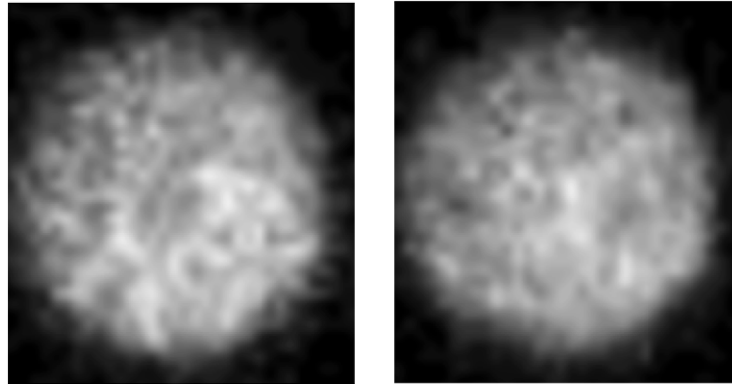
Fig. 2. Two views of Ceres as observed by Hubble Space Telescope (J. Parker personal communication, 2000).

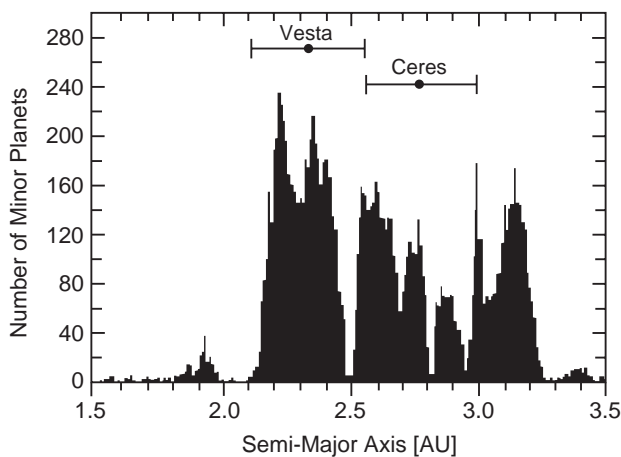Fig. 3. Number of asteroids vs. semi-major axis in astronomical units with the range of heliocentric distances over which Vesta and Ceres travel.

Table 1
Recent radius determinations of Ceres

Technique	Equator (km)	Polar (km)	References
Stellar occultation	480 ± 2	453 ± 5	Millis et al. (1987)
HST/FOC	485 ± 5	466 ± 6	Parker et al. (2002)
Adaptive optics	508 ± 5, 473 ± 7	445 ± 5	Drummond et al. (1998)
Adaptive optics	499 ± 20	469 ± 20	Saint-Pe et al. (1993)
Average	489 ± 6	458 ± 6	

culated geometric albedos of 0.056 near-UV ($\lambda=363.6$ nm), 0.029 mid-UV ($\lambda = 279.5$ nm), and 0.090 far-UV ($\lambda = 162.1$ nm). Tedesco et al. (1989) gives a visual albedo of ~ 0.10. Radar observations indicate Ceres is smoother than the Moon at decimeter wavelengths but much more irregular at longer wavelengths (Mitchell et al., 1996). From passive microwave observations Webster and Johnston (1989) suggested that Ceres is covered with dry clay-like material at least 3 cm thick.

The reflectance spectrum of the integral disk of Ceres is relatively flat and featureless (e.g. Gaffey and McCord, 1978; Bell et al., 1989; Bell, 1995; Gaffey et al., 1993a, b) but there is a UV absorption band and there is an absorption near 3 μm that has been interpreted as indicative of hydrated minerals (Lebofsky et al., 1981). However, although less likely, this absorption feature has also been attributed to ammonia-bearing clay, possibly ammoniated saponite (King et al., 1992) or ammoniated montmorillonite (Rivkin, 1997), implying temperatures of < 400 K since the surface minerals formed. A'Hearn and Feldman (1992) reported evidence for the escape of OH from the northern limb, consistent with a model in which a winter polar cap is replenished by subsurface percolation that dissipates in summer. Modeling studies using the OH evidence by Fanale and Salvail (1989) suggested water ice could be preserved within 10–100 m of Ceres' surface for the age of the solar system.

In the end, though, unlike Vesta, we cannot link any known meteorites to Ceres (e.g., Burbine, 1998; Sato et al.,

From bulk density can be drawn some inferences about the general composition of the asteroid. Ceres is similar in density to the two outer Galilean satellites, Ganymede and Callisto. These two objects are less evolved than the inner Galilean satellites, Europa and certainly Io, and are thought to contain considerably larger amounts of water. Vesta is considerable more dense and is known to be highly thermally evolved. 2 Pallas is also denser, but the reason (thermal evolution or low water at birth) presently is unclear. Britt et al. (2002) discuss at some length the topic of asteroid densities in general, although concentrating on the smaller objects where porosity can be significant. Thus, Ceres seems wetter and less evolved, more like Callisto or Ganymede than Vesta or Europa.

The surface composition of Ceres' surface has been suggested at times to be most similar to but not exactly like carbonaceous chondrite-like material (e.g., Gaffey and Mc-Cord, 1978; Larson et al., 1979), from its relatively flat spectrum and suggestions of the presence of water, but with a higher albedo. Millis et al. (1987) reported a V($\lambda = 560$ nm) geometric albedo of 0.073. Parker et al. (2002) cal-

1997). It is possible that Ceres is covered by a veneer of material that does not survive meteorite-producing impacts or terrestrial atmospheric passage. It is also possible, even likely (McCord and Sotin, 2003), that thermal evolution of Ceres has produced a metamorphosed carbonaceous chondrite surface material, such as containing hydrated salt minerals that produce higher albedos than for normal carbonaceous chondritic materials. In any case, Ceres is a mysterious and perhaps unique object in the solar system, but probably representative of some of the earlier objects that formed the major terrestrial planets.

3. Mission overview

Dawn is presently scheduled to be launched on a Delta 2925H launch vehicle from the Eastern Test Range in late May or early June 2006 on a direct trajectory to Vesta (Fig. 4) arriving at Vesta at the end of July, 2010. Ion propulsion is used during the interplanetary cruise to match trajectories with the asteroid. A slow approach ensures there are no time-critical thruster firings for orbit insertion. Insertion is completed using the ion propulsion system.

On approach, Dawn completes a survey of the region around Vesta for satellites, dust and debris and then moves under SEP thrust to its polar optical mapping orbit at 700 km altitude where it obtains measurements with the camera and the mapping spectrometer in a nadir pointing orientation. During science operations and data transmission the thrusters are off. Momentum wheels maintain attitude and hydrazine burns execute any emergency maneuvers.

Dawn plans to operate at Vesta for 11 months (7 in science operation, 4 under thrusting), acquiring imagery with illumination over both poles and precise elemental composition measurements. In Fig. 5 the top panel shows the latitude of the subsolar point over the course of the stay at Vesta. Varying sun angles provide illuminations of first the northern and then the southern hemispheres. Interest is very high in the southern polar regions where the large crater visible in Figs. 1 and 4 has excavated deep into the differentiated interior. The bottom panel shows Vesta's heliocentric distance during this period. This period coincides with perihelion and the highest possible ion thrusting levels. Later departures from Vesta will result in lower possible thrust levels.
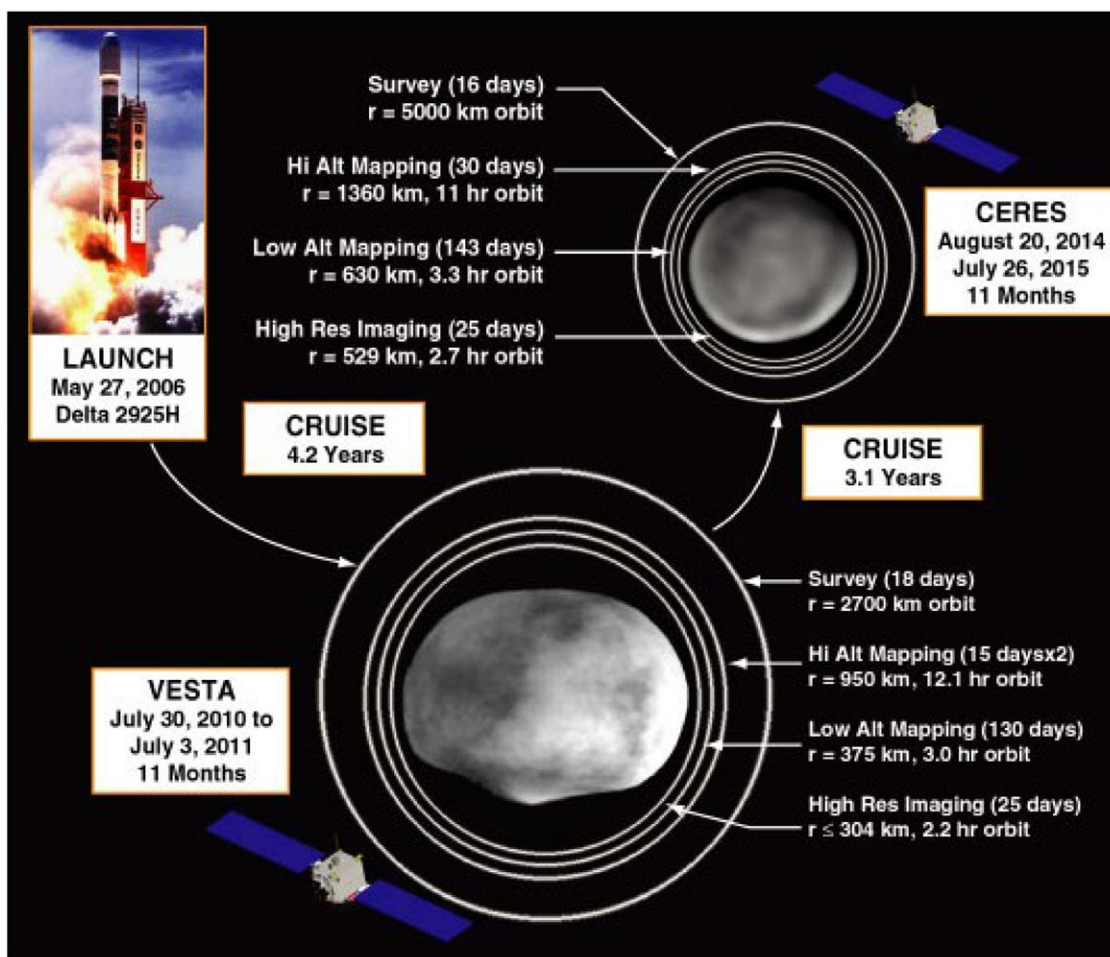

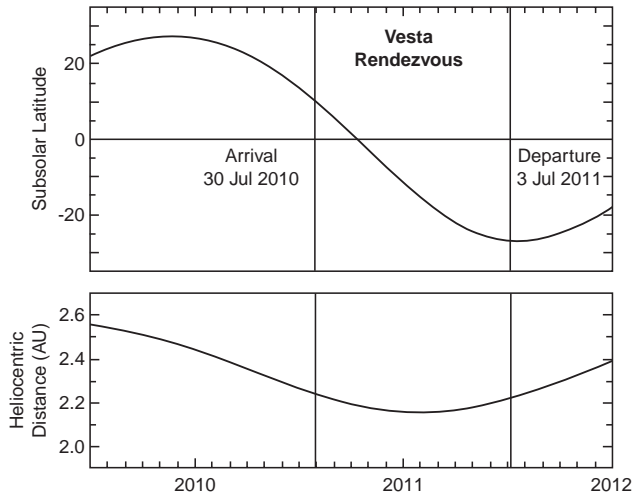Fig. 4. Pictorial summary of the Dawn mission.

Fig. 5. (Top) Subsolar latitude during Dawn planned operations at Vesta (Bottom) Heliocentric range.
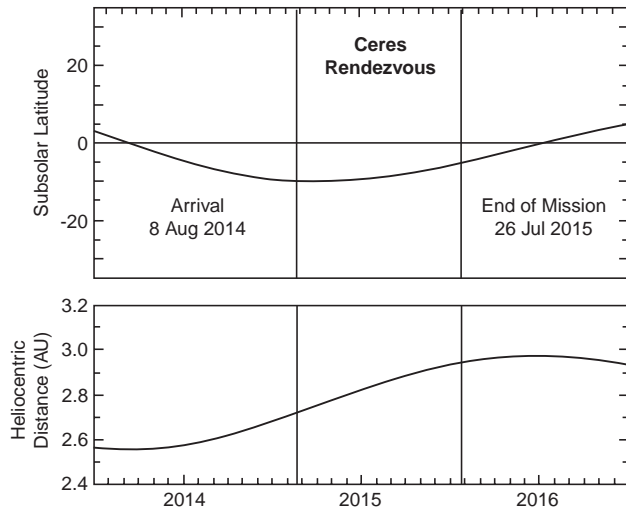

Fig. 6. Subsolar latitude during Dawn planned operations at Ceres.

After completing the high-altitude optical survey, the spacecraft uses SEP again to descend to the low altitude mapping orbit of 130 km altitude, where it obtains magnetic field and topography data and gamma ray and neutron spectroscopy. A further descent for a month to a lower altitude is made if safe. Each orbit has a prime instrument objective and there is no contention for spacecraft pointing or telemetry, simplifying sequencing. After 6 months at low altitudes SEP raises the spacecraft to 700 km again to obtain imaging and spectroscopy, complementary to that obtained immediately upon arrival.

Present plans call for Dawn to leave Vesta in July, 2011, and to proceed via ion propulsion to Ceres, arriving in August, 2014 repeating the same sequence of observations. As indicated by Fig. 6, the southern pole is illuminated upon arrival with increasing northern illumination with time. The

Table 2
Examples of the many flyby opportunities along Dawn's flight path

Body	Radius (km)	Rel. Vel. (km/s)	Distance (Gm)	Date (mo/year)
197 Arete	15	2.1	3.2	3/12
14924 1994VZ	2.2	3.5	4.5	3/09
18272 2495 T-3	1.1	3.4	2.1	7/09
20484 1989 NL41	2.5	1.9	4.0	10/11

mission is scheduled to end in July, 2015. The bottom panel of Fig. 6, shows the heliocentric range of Ceres. Since Ceres is receding with time, power available for thrusting is decreasing and any mission delays risk mission completion as the thrusters become less efficient. A possible solution to this problem is to delay arrival at Ceres until it is well past aphelion. Whether such options have to be considered await further testing and knowledge of the final spacecraft mass, that will not be known until much later in the project.

During the cruise to Vesta and from Vesta to Ceres the trajectory can be minimally altered to pass arbitrarily close to a number of asteroids, a selection of which are shown in Table 2, listing the flyby distance prior to any orbit adjustment. Owing to the efficiency of SEP, the number of candidate flyby targets is expected to be large with many opportunities for low-velocity encounters. Groundbased observations of these targets will be critical to a selection of targets on the basis of science return as opposed to simple dynamical convenience.

Dawn carries four instruments: a framing camera (FC), a visible—IR mapping spectrometer (MS), a gamma ray and neutron spectrometer (GR/NS), and a magnetometer (MAG). It also obtains radio science data to determine the asteroids' gravity fields. A fifth instrument, a laser altimeter, was dropped during Phase B when its expected costs rose well above the amount budgeted. As illustrated in Fig. 7 the instruments are body-mounted on the nadir-facing panel of the spacecraft with no articulation. The magnetometer does not require pointing control. In each orbital phase, one instrument controls the pointing (Table 3). In the optical mapping orbit, spacecraft pointing is determined by the needs of the framing camera, which views 5300 km^2 at a resolution of 69 m/pixel. Short exposures are used to avoid image blur. Pointing is nadir, except for targets of opportunity for the camera. Over a 30-day period, the entire surface of Vesta (and Ceres) will be mapped twice in each of seven filters under different lighting conditions (Table 4). Solar phase angles as small as 20° are obtained in this orbit at an angle ideal for the mapping spectrometer, scanning the entire surface at a resolution of 170 m/pixel. High solar phase angles, best for the framing camera, are principally obtained in the second optical mapping period near departure. The spacecraft then uses ion propulsion to descend to a polar, 130-km altitude,
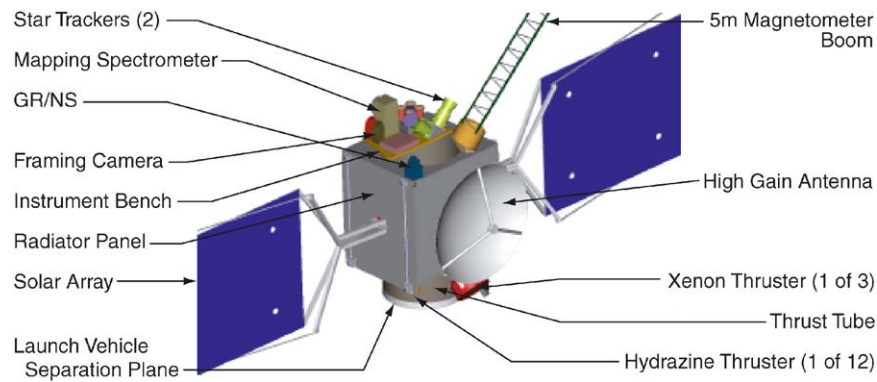
Fig. 7. Dawn spacecraft and payload. Note that the solar array and the magnetometer boom have been cropped.

Table 3
Orbital parameters at Vesta and Ceres. For each phase, one instrument controls pointing and there is no contention for spacecraft attitude

Body	Period (h)	SMA (km)	Altitude (km)	FOV[a] (km)	Pixel[a] (m)	Pointing optimized for
Vesta	12.1	950	661–721	69	68	Optical mapping[b]
	3.0	375	86–146	12	12	Topography[c]
	2.2	304	15–75	5	5	Hi-res imaging[d]
Ceres	11.0	1360	880–906	89	89	Optical mapping[b]
	3.3	610	130–156	14	14	Topography[c]
	2.7	529	49–75	6	6	High-res images[d]

[a] Framing camera.
[b] Visible and IR.
[c] Gamma-ray and magnetic field included.
[d] Shared control but generally nadir pointing.

Table 4
Images obtained in each phase of the mission

Phase	Framing camera					Mapping spectrometer	
	Res (m)	Clear images	% surface	Filtered images	% surface	Res (m)	2-Dim. spectra
Cruise 1[a]	NA[a]	7000	NA	0	NA	NA	0
V Survey	250	2180	NA	0	NA	NA	0
V Optic Map	69	1200	700	600[b]	350	140	7100
V Hi Res Map	5	2400	15	0	NA	10	3500
Cruise 2[a]	NA	7000	NA	0	NA	NA	0
C Survey	450	2650	NA	0	NA	NA	0
C Optic Map	89	1518	430	759[c]	216	178	5500
C Hi Res Map	6	2500	7	0	NA	12	3650

NA—Not applicable.
[a] Excluding targets of opportunity.
[b] In each of 7 colors.
[c] In each of 3 colors.

mapping orbit. This orbit is used to determine topography and shape of the asteroids, develop a comprehensive gravity field up to 12th degree at both Vesta and at Ceres, to measure the magnetic field of the body (MAG), and to determine its elemental composition (GR/NS). The magnetometer covers the asteroids with mapping tracks on the average of 0.4 km apart at the equator on Vesta and 1.0 km at Ceres, much more than is needed to resolve any remanent field present. Once the gravity field is known and it is safe to proceed, a lower altitude high-resolution mapping orbit is entered providing a resolution of 5 m/pixel. GR/NS has a 2 steradian field of view and a spatial resolution comparable to its altitude

Table 5
Dawn telemetry requirements by phase

Phase	Duration (days)	Total science bits (Gbits)[a]				Track. h/week		Tele. margin
		FC	MS	GR/NS	MAG	NAV	Telem.[b]	%
Cruise 1	1525	18	—	—	—	4	3.5	14
V Survey	18	5.6	—	—	—	112	17	686
V Opt Map	30	13.2	12	4.8	1.6	56	40	40
V Low Alt	130	14	—	29	9.7	24	17.5	37
V Hi Res	25	9	6	6.5	2.2	56	36	55
Cruise 2	1144	18	—	—	—	4	3.7	10
C Survey	16	5	—	—	—	112	11	935
C opt map	30	9.3	9.3	4.9	1.6	56	44	27
C Low Alt	143	18	—	37	12	24	17.5	37
C Hi Res	25	9	6.2	6.5	2.2	56	36	55

[a] Assumed compression ratios: FC 6:1, MS 2.5:1.
[b] Include 1 kbps engineering data and 15% relative overhead in downlink.

above the surface. The GR/NS obtains 5 months of medium and low altitude data at Vesta and slightly more at Ceres, enough to resolve all major elements and to spatially resolve the most abundant elements with a resolution that will depend on that abundance. At the end of the high-resolution mapping at Vesta, Dawn returns to the high altitude mapping orbit and remaps under yet different illuminations and stereo angles. At Ceres the nominal mission ends at low altitudes.

3.1. Data return

The data are stored for later transmission at 64 kbps (2 Gbits in 8.6 h). Dawn has a 64-kbps data rate out to 3.5 AU with 3-db link margin and can transmit at 128 kbps inside 2.5 AU. In sizing the telemetry needs we have conservatively used the 64-kbps rate. The weekly telemetry requirements (Table 5) indicate that the data buffer should be dumped only 1–5 times per week even at the most active times. In order to provide radiometric tracking for navigation as well as telemetry downlink, we have scheduled from 24 to 56 h of tracking per week in orbit and 4 h/week in cruise. In all mission segments, the downlink time required for navigation exceeds that needed by the science telemetry and by the field studies. Since telemetry is transmitted simultaneously with navigation tracks, Dawn has no contention for bits and has a flexible response to serendipitous discovery.

3.2. Performance floor

In the Discovery program each mission has a cost cap that triggers descopes when unexpected expenditures approach the cost cap. Furthermore, each mission is required to define a performance floor beyond which it may not pass without being terminated. Dawn's performance floor mission preserves many of the objectives of the baseline mission

Table 6
Baseline/Floor Mission Comparison. The performance floor mission performs a rendezvous with Vesta only and lasts 5.3 years

	Baseline Mission	Performance Floor
Launch Date	May 27, 2006	May 27, 2006
Targets	Vesta, Ceres	Vesta, 50 Virginia[a]
Mission End Date	July 26, 2015	September 16, 2011
Mission duration	9.2 years	5.3 years
Time in orbit (days)	338 (V) + 340 (C)	426 (V)
Fuel Used (Xe)[b]	428 kg	380 kg
Dry mass[b,c]	680 kg	615 kg
Hydrazine[b,c]	56 kg	27 kg

[a] Candidate.
[b] Including reserve and margin.
[c] For maximum injection mass.

(Table 6) with a reduced instrument complement and relies on a flyby to obtain the contrasting asteroid data. The framing camera and mapping spectrometer, the gamma ray/neutron spectrometer and radio science probe, explore a complementary asteroid, possibly 50 Virginia, a 100 km diameter Ch asteroid (indicating possible hydration processes), similar in spectral class to Ceres. This descoped mission provides mass, shape, volume, mineral (but not elemental) composition, information on surface processes and the role of water on the surface of the flyby asteroid. Dawn then orbits Vesta for 14 months (12 for science data) providing all the measurements of the baseline mission except the magnetometer data. The mission relies on optical tracking of features to obtain the nutation measurements necessary to deduce internal structure and constrain the size of any metallic core. Constraints on thermal evolution rely solely on optical and mineralogical data and not remanent magnetization. A longer (by 3 months) stay improves the topological data and increases the spatial and elemental abundance resolution obtained with the GR/NS. Questions directly related to Ceres are not addressed in the descoped mission unless Ceres is the flyby target. Table 5 compares

the baseline and performance floor mission scenarios. Savings in mass occur because of the smaller instrument complement, one less thruster and less fuel. Reduced operations provide the principal cost savings.

4. Measurements

4.1. Imagery

Imagery contributes to many of Dawn's science objectives, often in combination with other data sets. For example the average density is calculated from the volume derived from images and the mass from radio science. The prime task for the camera is to decipher the geologic history and evolution of the asteroids by characterizing and mapping their surfaces. To do this, they are observed with a high-resolution spectral camera (0.4–1 μm) at varying distances from far-field global maps to local-site characterization under various observing geometries and lighting conditions. The analysis of geomorphologic features (down to the scale of a few meters in the high resolution phase) yields unique evidence on the different geologic processes responsible for the state of the asteroidal surfaces like volcanism, impact processes, water mobilization, and weathering. Clues to the formation age of the entire asteroid and its stratigraphy can be derived from the frequency-size distribution of craters, their morphology and interior structure. The vertical accuracy of the stereo data is similar to the spatial pixel resolution. Multispectral images allow mapping compositional units while multi-angle images provide hints to the textural properties of the asteroidal regolith and the surface roughness. The filter pass bands are optimized for the electronic absorption band in Vesta's spectrum as shown in Fig. 8. We expect to use only three of these bands at Ceres.

The one clear and seven color filters take into account the spectral reflection characteristics of Vesta which is dominated in the visible/near IR wavelength range by a reflection maximum around 750 nm, a slope towards the ultra violet, and a characteristic absorption at 1000 nm due mostly to Fe^{2+} in the mafic mineral pyroxene (McCord et al., 1970). Spectral observations from Earth reveal at least three different surface units (Gaffey, 1997) with a composition similar to eucrites, diogenites, and a smaller-sized patch (possibly a crater) similar to dunite, an olivine-rich assemblage. Discrimination between surface lithologies requires a good description of variations within the UV-slope as well as of the 1000 nm-absorption band. The color filters address these tasks. The one at the reflection minimum provides high sensitivity for distinguishing compositional units. The seven filters are centered at 430, 540, 650, 750, 830, 920 and 980 nm. They detect:

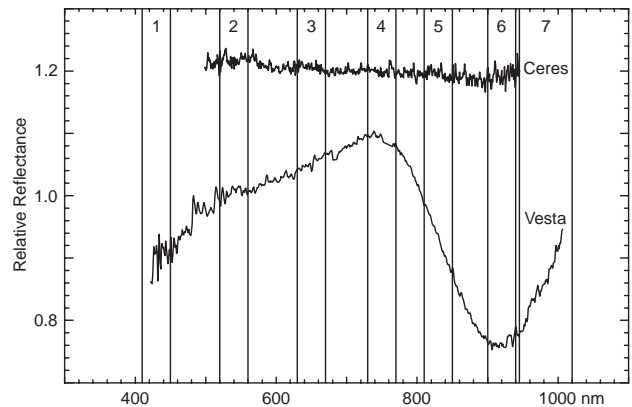1. The edge of the UV absorption.
2. Slope variations.

Fig. 8. Ceres and Vesta reflectance in the visible and near infrared with filter bands of the framing camera superimposed.

3. Slope variations and a possible shift of the reflection maximum toward shorter wavelengths (i.e. due to olivine).
4. The maximum reflectance.
5. The bandwidth of the 1000 nm absorption and the presence of olivine (Fe^{2+} in the M1 position of olivine).
6. The absorption maximum of pyroxene for Vesta located between 910 and 930 nm.
7. Broadening of the 1000 nm absorption due to variations in pyroxene composition and/or the presence of olivine.

The color filter at 830 nm allows for matching the high spatial-resolution color images with the visible and infrared reflectance spectrometer data. The camera is also used for optical navigation. At a distance of 10^7 km, a 0.1-s clear exposure detects either asteroid with signal-to-noise ratio larger than 100. The expected positioning accuracy is of the order of 10^{-5} radian. More images are needed at Ceres to characterize its greater surface area, but fewer filtered images are needed because of its flatter spectrum.

4.2. Framing camera

Two identical framing cameras, to be designed and built by MPAe Germany in co-operation with DLR Berlin and IDA Braunschweig will provide images of the surface of the target asteroids and will be used for navigation. The camera (see Fig. 9 for preliminary drawings of camera head and electronics box) uses an f:1/8 rad-hard refractive optics with a focal length of 150 mm. The field of view of $5.5° \times 5.5°$ is imaged onto a frame-transfer CCD with 1024×1024 sensitive pixels. With a pixel pitch of 14 μm the camera samples the scene at 9.3 m/pixel from a distance of 100 km. Two identical camera systems including data processing units will be delivered to provide redundancy for optical navigation. One camera head consists of the housing, refractive lens system, filter-wheel, focal plane, and readout electronics with 2.5 kg total mass and 1.8 W power consumption.
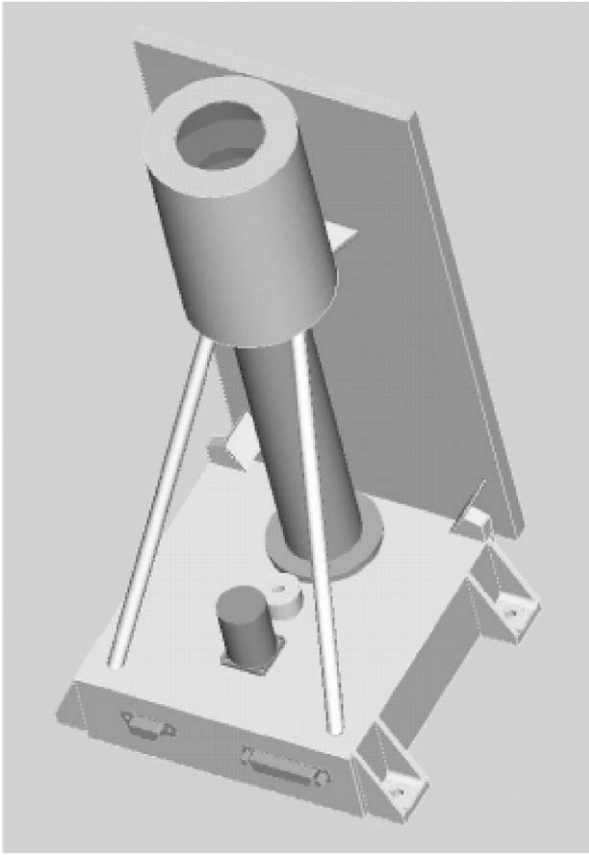
Fig. 9. The sensor head of the framing camera.

The data processing unit controls the camera and handles the data by compressing and buffering them. Data compression of the 14-bit samples is implemented by software based on wavelet algorithms. Compression rates can be selected from lossless (about 2:1) to lossy 10:1 (and more) for which still acceptable images are provided.

The filter wheel has eight positions and is equipped with one clear filter and seven multispectral filters. The clear filter is used to support spacecraft navigation and for high signal-to-noise (SNR) observations, e.g., imaging at exposure times much less than the dwell time to enhance image contrast and sharpness of morphologic features, searching for dust at forward scattering observation geometries as well as high-speed imaging during the closest approach of additional asteroidal flybys. Except for the clear filter covering the range 450–950 nm and the 980 nm filter with a full-width-half-maximum (FWHM) of 80 nm, all spectral channels have 40 nm FWHM. The sensitivity is sufficient for the surfaces of Vesta and Ceres to be imaged in each filter with a SNR of 100 for exposures from 100 ms to 1 s. At lowest altitudes when blur might occur in longer duration color exposures the clear filter and shorter (25 ms) exposures are used. A stray light baffle shades the pupil from reflections from the spacecraft body and allows imaging as close as 20° sun avoidance angle.

The camera operates at a readout rate of 650 k pixel/s or 1.6 s per 1024×1024 frame. The minimum exposure time is 1 ms. To improve the SNR data, pixels can be binned under software control on the CCD or subarrays selected to increase the read out frame rate. The digital processing unit has 16 Gbit of gracefully degrading instrument related memory equivalent to 1000 uncompressed pictures. Each DPU consumes between 2 and 5 W and weighs 2.5 kg. The total resources per camera are 5 kg of mass and circa 12 W consumption. A keep alive line ensures storage of the images for extended times while the rest of the camera is turned off. A reclosable cover is used in front of the optics to protect against contamination from external sources. Dedicated heaters on the focal plane detectors are used to drive off possible condensing contaminants, to provide for annealing of the detector to reduce radiation damage, and to maintain favorable temperature gradients during long cruising intervals. The command software is high level and based on the operating system developed for OSIRIS (Science imagers for the Rosetta mission) and VMC (Venus Monitoring Camera).

The design of the camera is based on several lines of heritage. The DPU is essentially a copy of the unit for VMC on VENUS EXPRESS that will be delivered early 2004. In particular the software will be the same as developed for OSIRIS and VMC with very minor adaptations for DAWN. The optical design is conservative and promises excellent performance based on the detailed phase A study. The detector and read out electronics are a copy of the units implemented in the ROLIS Down-looking Imager on the ROSETTA lander. There are two mechanisms: a filter wheel operated by a Geneva-type drive is currently breadboarded and will be in test from the end of June on. The lightweight plane filter wheel itself will be based on a design flown in the Halley Multicolour Camera of the GIOTTO mission. A similar drive concept (but reciprocating) was built by MPAE for the protective cover drive of the optics in the Robotic Arm Cameras of the Mars Polar Lander and the 2001 Mars Surveyor Lander. The optics cover is under design and will incorporate a fail safe release mechanism. Both mechanisms will be driven by identical stepper motors; motors of the same type (but larger) were successfully flown on missions like SOHO. MPAE has more than 20 years of experience in designing, manufacturing, and qualifying of complex mechanisms for interplanetary space missions.

4.3. Mineralogy

A prime objective of Dawn is to determine the mineral composition of the surface and to place it in geologic context. The nature of the solid compounds of the asteroids (silicates, oxides, salts, organics and ices) can be identified by visual and infrared spectroscopy using high spatial resolution imaging to map the heterogeneity of asteroid

surfaces and high spectral resolution spectroscopy to determine the composition unambiguously. The first use of spectroscopy to determine the composition of an asteroid was for Vesta (McCord et al., 1970). A variety of diagnostic absorption bands for key minerals occur in the visible and near-infrared and can be identified with spectroscopic measurements (e.g. Burns, 1993; Gaffey et al., 1993a, b). The olivine exhibits an asymmetric feature, a combinations of three overlapping absorptions, near 1 μm. The orthopyroxene spectrum shows two symmetric features near 1 and 2 μm. Feldspar has a weak band near 1.25 μm from its trace content of Fe^{2+}. Absorption band position is also diagnostic of the specific mineral chemistry. The substitution of a large cation for a smaller one expands and distorts the entire crystal structure, giving origin to diagnostic absorption bands.

Well detectable in the visible are also charge transfer absorptions involving electronic transitions between different shells or between adjacent cations. These generally occur at shorter wavelengths and are significantly stronger than the crystal field absorptions. The overlapping of several of series of charge transfer features gives rise to the strong blue-ultraviolet absorption edges in many silicates (in the region < 0.7 μm).

Water vibrations around 2.84 and 3.05 μm are combined to give a large and strong feature around 3 μm in asteroidal spectra. The presence of this feature at 3 μm in asteroidal spectra is indicative of a water-bearing phase such as hydrated silicates. In particular, the presence of the 1.4 and 1.9 μm bands is indicative of H_2O molecules, while the existence of 1.4 μm feature alone suggests OH groups in minerals. The carbonate minerals could be concentrated wherever aqueous alteration has taken place on asteroids. Weak absorptions bands are identified in reflectance spectra of some dark asteroids, suggesting that these features are due to iron oxides in phyllosilicates formed on asteroidal surface by aqueous alteration processes (Vilas and Gaffey, 1989) (Fig. 9).

Shown in Fig. 10 are reflectance spectra of minerals typical of asteroids and meteorites (Pieters and McFadden, 1994). Common rock-forming minerals in both meteorites and asteroids exhibit distinctly different and diagnostic absorption bands. The wavelength, shape and strength of various absorption features are determined by the minerals present. Each parameter must be measured accurately to make identifications and derive relative abundances. The mapping spectrometer has the resolution and accuracy necessary for this inversion process. Methods for compositional information extraction range from straightforward linear or nonlinear mixing models of multiple components to a more sophisticated quantitative analysis of individual absorption features (see summary in Pieters et al., 1996). Maps of the current surface mineralogy together with studies of cratering that excavates and redistributes materials lead to an understanding of the evolution of the surface and determine the processes affecting it.
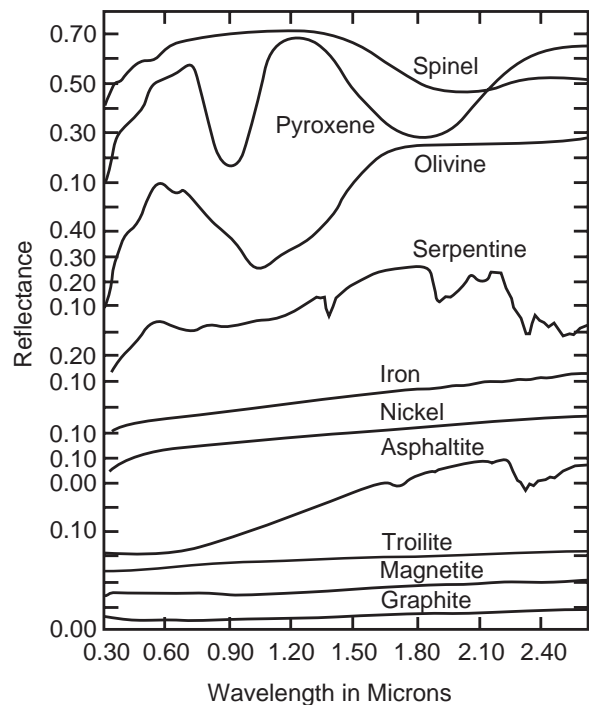

Fig. 10. Reflectance of different materials illustrating the variation in absorption features in different materials (Pieters and McFadden, 1994).

Medium resolution spectral images in the visible and infrared regions reveal information on the mineralogical composition of the asteroid surface. Simultaneous spectral resolution and spatial resolution are needed to investigate surface geology, making possible the identification of mineralogical provinces, and producing compositional maps. Such maps will provide information on the relationship between global and local spectral characteristics.

The Dawn Mapping Spectrometer covers the spectral range from the near UV (0.25 μm) through the near IR (5 μm) and has moderate to high spectral resolution and imaging capabilities. These characteristics make it an appropriate instrument for determining the asteroid's global surface composition. Fig. 11 shows Vesta's reflectance spectrum with deep absorption bands that are diagnostic of the mafic silicates present on its surface. Laboratory calibrations of controlled mixtures are expected to allow us to determine the chemistry of the pyroxene and olivine minerals at Vesta, using observations with Dawn's spectral resolution of $\Delta\lambda/\lambda = 0.01$–$0.002$ in the 1–5 μm region.

Fig. 12 shows the spectrum of Ceres (Rivkin, 1997). It is relatively flat shortward of 2.5 μm, with strong features longward of 2.5 μm, attributed by some to ammoniated phyllosilicate. An Fe charge-transfer feature at 0.7 μm (not shown) also arises from phyllosilicates (Vilas and Gaffey, 1989) which originated from aqueous alteration processes Vilas, 1994). This feature is weak on Ceres (Vilas and Gaffey, 1989), indicating iron-poor minerals or heating
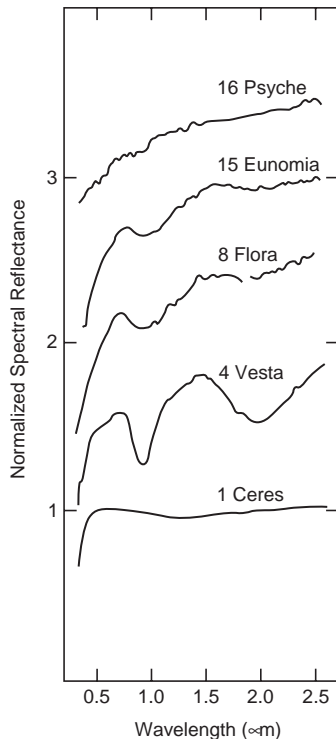
Fig. 11. Normalized reflectance spectra of major asteroids. Figure from "Reflectance spectroscopy and surface mineralogy" by Gaffey, Bell and Cruikshank edited by Binzel, Tom Gehrels and Mildred Shapley Mathews. © 1989, The Arizona Board of Regents. Reprinted by permission of the University of Arizona Press.
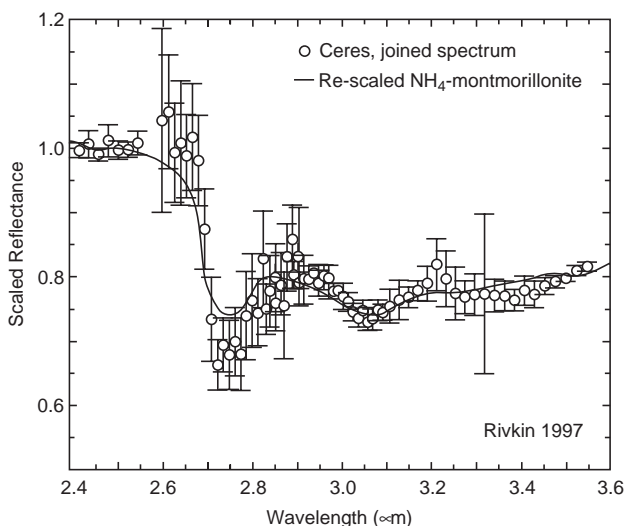

Fig. 12. Spectrum of Ceres illustrating absorption near 3 µm (Rivkin, 1997).

above 400°C (Hiroi et al., 1993). However, this is constrained by the presence of ammoniated phyllosilicate, which is destroyed at temperatures above 400°C. Clay formation may have arisen from the mobilization of water from internal heating or by cratering (as one of the oldest

surfaces in the asteroid belt, the surface of Ceres is expected to be heavily cratered). It is not known whether some or all of Ceres' surface will answer this question. Spatially resolved spectra of Ceres over the 0.7 µm feature, combined with maps of elemental abundance determined by GR/NS, including Fe, will give us the opportunity to distinguish between surface materials that have undergone aqueous processing, and unaltered source material that may be exposed at the surface. We may find that the spatial resolution of the GR/NS is not adequate to fully resolve exposed regions; however, depending on the contrast in composition between the processed and unaltered materials, it still may be possible to separate out their respective contributions. In addition, spatially resolved spectra of Ceres out to 5 µm and comparison with hydrogen data from GR/NS will allow us to identify a broad range of hydrated minerals and their distribution, providing further insight into the role of water in the thermal and geological evolution of Ceres and the conditions in the early solar system under which these processes occurred. Such spectra for both Vesta and Ceres, within craters and fissures, will reveal the compositional details of any underlying stratigraphy (and perhaps reveal any meteorites in our collections from Ceres).

In short, mineral identification using the location and depth of absorption features in the reflectance spectrum allows us to test existing hypotheses. We also determine the physical microstructure and nature of the surface particles. At Vesta we will test the link between Vesta and the HED meteorites. We will obtain the first in-depth view of a planetary interior through the spectral imaging of Vesta's wide and deep impact basin. We reveal the nature of Vesta's ancient magma ocean or volcanic emplacement history. We determine the mineralogy of a protoplanet that has remained at its formation location. Further we establish the abundances and mineralogy sufficiently to establish the source of meteorites recovered on Earth. At Ceres we investigate its primitive surface mineralogy. We identify water-bearing minerals and dry clay-like materials. We identify water-bearing minerals and clay-like minerals, and map surface ices or frost-covered regions. Finally, we expect to be able to detect any weak atmosphere.

4.4. Visible and infrared mapping spectrometer

The Dawn mapping spectrometer (MS) is a modification of the VIRTIS mapping spectrometer (Coradini et al., 1998; Reininger et al., 1996) on board the ESA Rosetta mission. It will be operated for 2 years and spend 9 years in space. It derives much design heritage from the Cassini VIMS spectrometer with an operational lifetime of > 4 years and a mission life > 10 years. The design fully accomplishes Dawn's scientific and measurement objectives. The design uses a dual arm optical and focal design with mapping capability to 5 µm. The mapping spectrometer is an imaging spectrometer that combines two data channels in one
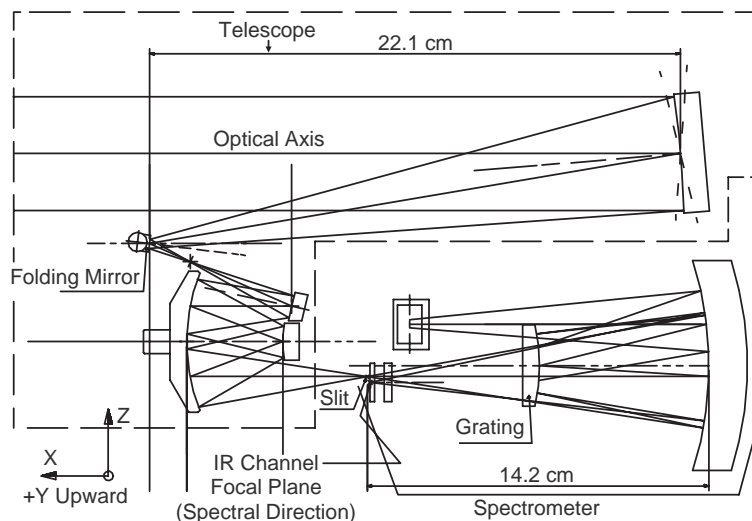
Fig. 13. Optical layout of the visible and infrared mapping Spectrometer.

compact instrument. The visible channel covers 0.25–1.0 μm and the infrared channel covers 0.95–5.05 μm. The use of a single optical chain and the overlap in wavelength between the visible and infrared channels facilitates intercalibration. It utilizes a silicon charge coupled device (CCD) to image from 0.25 to 1 μm and a mercury cadmium telluride infrared focal plane array (IRFPA) to image from 1 to 5 μm. The spectrometer consists of three modules: optical system (5.0 kg mass); proximity electronics (3.0 kg and 5 W); cryocooler including driving electronics (1.3 kg and 12.6 W). A mechanical and thermal mounting of 5.0 kg mass accommodates the spectrometer subsystems. The optical system, which includes foreoptics, dispersive elements, filters, focal plane assemblies as well as the cryocooler and proximity electronics is a complete re-build of the VIRTIS-M. The optical concept is inherited from the visible channel of the Cassini Visible Infrared Mapping Spectrometer (VIMS-V) developed at Officine Galileo and launched on Cassini in October 1997.

This concept matches a Shafer telescope to an Offner grating spectrometer to disperse a line image across two FPAs. The Shafer telescope is the combination of an inverted Burch off-axis telescope with an Offner relay. By putting an aperture stop near the center of curvature of the primary mirror, coma is virtually eliminated. The result is a telescope system that relies on spherical mirrors, yet remains diffraction limited over a large spectral range and the whole spatial direction. The horizontal field is realized by rotating the telescope primary mirror around an axis parallel to the slit. The Offner spectrometer is matched to the telescope, and does not rely on a collimator and camera objective. This is possible because both telescope and spectrometer are telecentric and the telescope has its exit pupil on the grating. The optical layout is illustrated in Fig. 13.

The spectrometer does not use beam-splitters. Two different groove densities are ruled on a single grating. The grat-

Table 7
Mapping spectrometer optical specifications

Parameter	Mapping spectrometer
Pupil diameter (mm)	47.5
Imaging F#	5.6 Vis and 3.2 IR
Etendue (m² sr)	3.6×10^{-11} V and 7.5×10^{-11} IR
Slit dimension	38 μm × 9.53 mm
Spectral range (μm)	0.25–1.00 (Vis) 0.95–5.05 (IR)
Field of view (FOV)	64 mrad(slit) × 64 mrad(scan)
Modulation transfer function (MTF) @ (cy/1 mrad)	> 50%
FWHM (Linear Spread Function (LSF) ⊗ slit ⊗ pix)	< 60 μm
Spectral resolution	100–500
Spectrometer magnification	1

ing profiles are holographically recorded into a photoresist and then etched with an ion beam. Using various masks the grating surface can be separated into different zones with different groove densities and different groove depths. The "V" regions, which make up the central 30% of the conjugate pupil area, correspond to the higher groove density needed to generate the higher spectral resolution required in the "visible" channel extending from the ultra-violet to the near infrared. The infrared channel utilizes the outer 70% of the grating, which is ruled with a lower groove density. The larger collecting area in the infrared compensates for the lower solar irradiance in this region. Table 7 lists the optics specifications.

The visible detector array is based on the Thomson-CSF type TH 7896 CCD detector. It uses a buried channel design and poly-silicon N-MOS technology to achieve good electro-optical performance. Moreover, it includes a multi pinned phase (MPP) boron implant to operate fully inverted and substantially to decrease the surface dark current, residual images after strong exposure and other effects due to

ionizing radiation. The TH7896M is a full frame image sensor with 1024×1024 sensitive elements, two registers and four outputs. It will be used as a frame transfer device with a sensitive area and a storage area. The first half is used to acquire the data and the second half is used to send the data to the proximity electronics to be converted.

The IR detector used in the spectrometer is based on a bidimensional array of IR-sensitive photovoltaic mercury cadmium telluride coupled to a silicon CMOS multiplexer. The device is an array of 270×435 HgCdTe photodiodes manufactured by Raytheon Infrared Center of Excellence (Santa Barbara USA) with a spacing of 38 μm between diode centers. The spectral wavelength range is 0.95–5.0 μm and an operating temperature of 70 K. The detector is packaged into a housing which includes an optical window which provides suitable mechanical, thermal and electrical interfaces for its integration on the focal plane. Furthermore, the window functions as substrate for the order-sorting filters. These filters are used to stop the superimposition of higher diffraction orders coming from the grating and also to reduce the background thermal radiation from the instrument housing. The transmission characteristics of the window are optimized for each corresponding detector position, so that for each filter zone only the designed wavelength range corresponding to the first diffraction order is allowed to pass. Six segment filters are coated in the window with the following bandpasses: 0.9–1.6, 1.2–1.9, 1.9–2.5, 2.4–3.75, 3.6–4.4, 4.3–5.0 μm.

In order to minimize the thermal background radiation seen by the IR-FPA, the spectrometer itself needs to be cooled to less than 135 K by radiating at least one, or possibly two of its surfaces toward cold space. Such a configuration also provides the operational temperature needed for the CCD. The IR-FPA requires an operating temperature of 70 K to minimize detector dark current, which is achieved by using a Stirling active cooler driven by dedicated electronics. The Stirling cooler that best meets MS requirements with off-the-shelf products is the RICOR K508 tactical cooler. It is an integral cooler in which the regenerator, where the heat exchanges at warm and at cold temperatures occur, is directly connected to the compressor. Without the transfer line characterizing the split cooler, less heat losses occur and more efficiency is reached. On the other side, due to the internal balancing device and the reduced heat flow from the compressor to the cold finger, vibration and heat transmitted to the regenerator and to the cold end (where the FPA is connected) are very limited.

A cover in front of the optics entrance aperture protects against contamination from external sources. Dedicated heaters on the focal plane remove possible condensing contaminants and provide for annealing of the detector to reduce radiation damage. The cover-inside is coated and used as calibration target in combination with two internal calibration lamps (one for the VIS-FPA and one for the IR-FPA).

4.5. Elemental composition

Planetary objects with thin atmospheres emit gamma rays with energies characteristic of the emitting nucleus through the decay of naturally radioactive elements, principally Th, U and K. Gamma rays also stem from nuclear reactions induced by neutrons generated by galactic cosmic ray interactions with the nuclear constituents of all matter, which for Dawn includes both the asteroids and the spacecraft. Underlying the gamma-ray line spectrum is a continuum coming from the asteroids, the spacecraft, and the galaxy. The gamma-ray/neutron data are obtained equally well for all solar lighting conditions and increase modestly with increasing heliocentric distance. With 130 days of observations at an altitude of 130 km or less above Vesta and Ceres, where the asteroid fills the GN/RS field of view (FOV), we measure the abundances of Fe, Ti, O, Si, Ca, U, Th, K, H, Al, Mg, Gd and Sm. This result holds both for the asteroids as a whole and separately within major geologic regions. This set constitutes all of the major rock-forming elements as well as several important trace elements.

Table 8 shows the expected statistical precision (ε), expressed as a relative standard deviation, for the determination of major—and radioactive elemental abundances for three different dry materials: eucrite, ferroan anorthosite, and basalt. Note that ε is expressed as a percentage of the listed abundance and is to be multiplied by, not added, to the percent abundances listed. The measurements are assumed taken over 120 h (5 days) at an orbital altitude of 130 km. The eucrite composition is representative of Vesta. The expected precision in elemental abundances for the eucrite composition indicate that the sensitivity of the GR/NS is sufficient to determine whether Vesta is the parent of the HED meteorites. The elements listed here constitute over 99% of the mass of HED meteorites and can all be detected in the expected stay times at Vesta and at Ceres. We create composition maps of both asteroids for latitude and longitude boundaries determined from the GR/NS measurements alone, as well as for geographical regions determined from the cameras. Since the asteroids fill the GR/NS FOV, its effective sensitivity greatly exceeds that obtained from NEAR at Eros at similar altitudes.

The neutron measurements enhance our ability to detect hydrogen and, by inference water, more than a factor of 3 in depth and a factor of 100 in concentration over that derived from gamma-ray analysis alone. A mass fraction of water greater than 0.02% can be detected at a neutron measurement sensitivity of 1%. This sensitivity is to be compared with the mass fraction of 3% H_2O contained in martian basalts. Neutron observations using the Lunar Prospector Neutron Spectrometer (which had a similar sensitivity to that for Dawn), yielded a hydrogen abundance of about 50 ppm near the lunar equator, 150 ppm near both poles, and 1700 ppm within the permanently shaded craters near the south pole of the Moon (Feldman et al., 2000). Dawn neutron measurements should therefore determine the

Table 8
Detectability of major elements

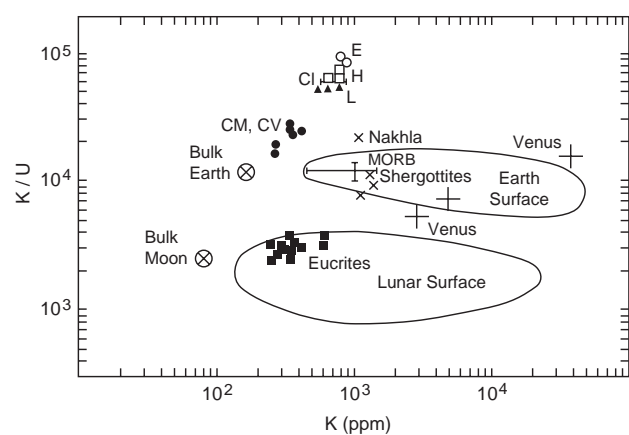|	Eucrite (Mason, 1979)		Ferroan Anorthosite (Lunar)		Hi-Ti Basalt (Lunar)	
	Abundance	ε (%)	Abundance	ε (%)	Abundance	ε (%)
O	42.4%	1.54	45.6%	1.35	41.5%	1.61
Si	22.8%	0.96	20.7%	1.09	18%	1.28
Ti	38%	0.28	0.08%	41.36	7.8%	1.00
Al	6.6%	5.41	17.6%	1.86	4.6%	8.01
Fe	14.6%	0.91	1.5%	2.47	14.2%	0.92
Mg	4.6%	4.13	0.5%	32.71	6%	3.22
Ca	7.2%	3.38	13.6%	1.81	7.4%	3.29
Th	0.45 ppm	5.29	0.8 ppm	3.12	10 ppm	0.27
U	0.1 ppm	17.47	0.3 ppm	5.95	3.7 ppm	0.51
K	400 ppm	4.79	200 ppm	9.32	3300 ppm	0.63

Fig. 14. Potassium to uranium ratio vs. potassium concentration (Taylor, 1992).

level of hydration of Ceres' crust. These measurements also provide an independent measure of the average atomic mass of surface soils, sufficiently robust to discriminate between basaltic and feldspathic lithologies.

A diagnostic indicator of the degree of volatile element depletion in planet-forming material in the inner solar system is the K/U ratio, measured by the gamma-ray spectrometer. Fig. 14 shows the K/U ratio plotted vs. K concentration for meteorites and lunar and terrestrial samples (Taylor, 1992). The meteorites clearly fall into specific classes in this display. Rocks from the surfaces of Earth, Venus, and Mars appear to be similar to each other and quite different from the various meteorite types and the lunar surface.

4.6. Gamma ray/neutron spectrometer

The Dawn gamma-ray and neutron spectrometer (GR/NS) maps the major (O, Si, Fe, Ti, Mg, Al, and Ca) and trace element (U, Th, K, H, Gd, Sm) composition. It draws on decades of experience at LANL in measuring neutrons and energetic photons and is an improved version of the

highly successful GR/NS on Lunar Prospector (LP), and the presently operating Neutron Spectrometer aboard Mars Odyssey (MO). The design of the spectrometer and its expected performance is described in detail by Prettyman et al. (2003). The gamma-ray sensor is segmented into two parts and the neutron sensor into four parts. Onboard classification of the multiple signals from each event then allows directionality determination that can discriminate radiation of asteroid and spacecraft origin. The gamma-ray sensor is a squared-off version of the LP scintillator, inlaid with a 4×4 array of 1 cm^3 cadmium zinc telluride (CZT) sensors on the side facing upward from the deck toward the asteroid. The CZT sensors are a new technology demonstration (Prettyman et al., 2002). This sensor is surrounded by four segments of an anticoincidence shield (ACS) made using a borated plastic scintillator (BC454). The upward (asteroid) and downward (spacecraft) facing segments of the ACS are laminated with an ^{6}Li loaded glass scintillator (GS20) to provide a separation between incoming thermal (GS20) and epithermal/fast (BC454) neutrons. The epithermal and fast neutrons are separated electronically as was done for the Lunar Prospector and Mars Odyssey instruments.

The Dawn GR/NS data at Vesta and Ceres are of comparable quality to that of the LP neutron spectrometers and have better than a factor of three higher spectral resolution than that of the LP gamma-ray spectrometer. Simulations verify that our present design provides a robust neutron and gamma-ray signal strength at Vesta and Ceres, adequately controls spacecraft backgrounds, yields a robust bismuth germanate (BGO) spectrum that is as good or better than that measured using the LP GRS BGO detector and is effective in suppressing the background from the spacecraft. If the CZT detector fails to achieve optimal resolution e.g. because of radiation damage in the space environment, the Dawn GR/NS science objectives are still met. We have shown that annealing of CZT at moderate temperatures (40–60°C) for short periods of time can fully restore resolution following radiation damage. The exposure predicted for the CZT behind the ACS is low enough that we do not anticipate significant degradation in performance due
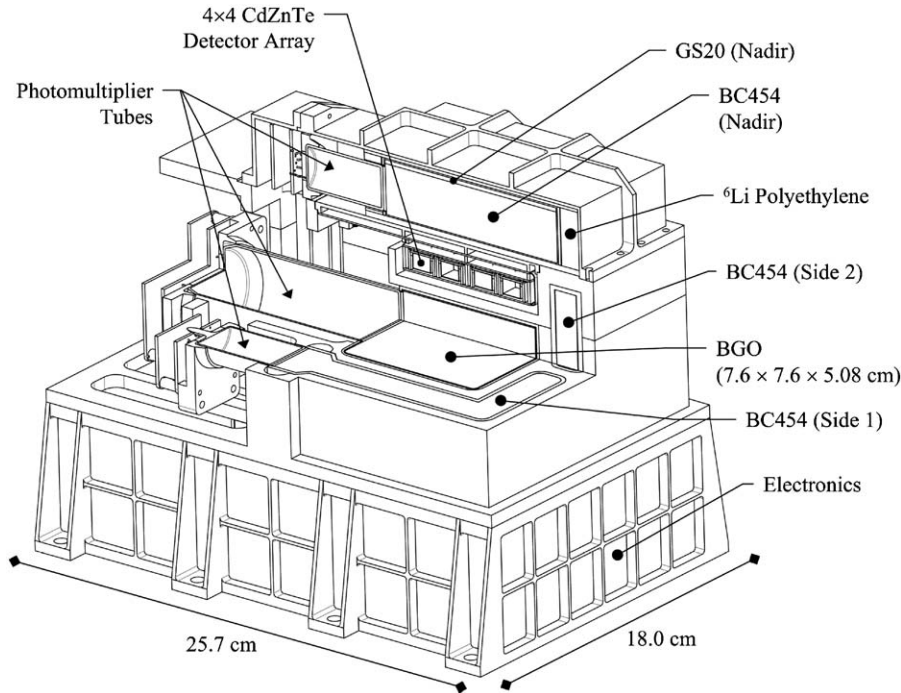
Fig. 15. Gamma ray/neutron spectrometer.

to radiation damage. However, to ensure performance, our design includes the capability to anneal the CZT array if damage is observed (Prettyman et al., 2003).

The Dawn GR/NS consists of a 7.6 cm wide ×7.6 cm long ×6 cm high rectangular slab of BGO that is viewed by a 7.6 cm diameter photomultiplier tube (PMT). A 4×4 square array of 16 cm^3 CZT sensor elements positioned above the upward BGO face (away from the spacecraft deck facing the asteroid) as shown in Fig. 15. The BGO acts as an active shield, minimizing spacecraft contribution to the response of the CZT array. This compound gamma-ray sensor is surrounded on five sides by a rectangular borated plastic ACS that is composed of four separate elements, each viewed by its own 2.5 cm diameter PMT. The thickness of each of the plastic scintillator elements is 2.5 cm. The top and bottom ACS elements are laminated by 2 mm thick lithium-6 glass scintillator sheets, which are viewed by the same PMTs that view the plastic to which they are optically coupled. The top and bottom ACS faces are surrounded on their sides by 1 cm thick sheets of ^{6}Li-loaded polyethylene to prevent access by thermal neutrons from the spacecraft.

The front-end electronics for the BGO and ACS portions of the GR/NS are configured to classify each detected event into one of five categories. These categories are identical to that used on LP and MO. The five categories are: (1) an isolated BGO interaction, (2) a single coincident BGO and ACS interaction, (3) a subset of these coincident interactions where the energy deposited in the BGO and BC454 are defined by window discriminators to fall within narrow ranges centered on 478 keV in the BGO and 93 keV in the BC454, (4) a single ACS interaction, and (5) a time-correlated pair of ACS interactions that occur within 25.6 μs. Addition of the CZT sensors adds four additional categories: (1) an isolated CZT event, (2) a coincident CZT and BGO interaction, (3) a subset of these coincident events where the energy deposited in the BGO is 0.511 ± 0.075 MeV, and (4) a coincident CZT and ACS interaction where the energy deposited in the CZT and BC454 are defined by window discriminators to fall within narrow ranges centered on 478 keV in the CZT and 93 keV in the BC454. Simulated spectra have demonstrated the capabilities of these hybrid CZT-BGO detector operation modes.

All information is packaged in a 3 kb/s data string with an accumulation time of 60 s. A 478 keV gamma ray from ^{7}Li* provides a continuous calibration of gain as proven on LP. Gamma-ray spectra, both accepted and rejected by the ACS are recorded separately and telemetered to Earth. Thermal neutrons from the asteroid are measured using the GS20 of the upward-facing ACS element and those from the spacecraft use the GS20 of the downward-facing element. Separation of the Li-glass from the BC454 will be implemented using time-domain filters that have been developed at Los Alamos.

Epithermal neutrons having energy in the range between about 0.2 eV and 0.5 MeV from the asteroid are measured using the BC454 of the upward ACS element in coincidence with a 478 keV CZT or BGO interaction. Those from the spacecraft use the downward ACS element in coincidence with a 478 keV BGO interaction. Fast neutrons having
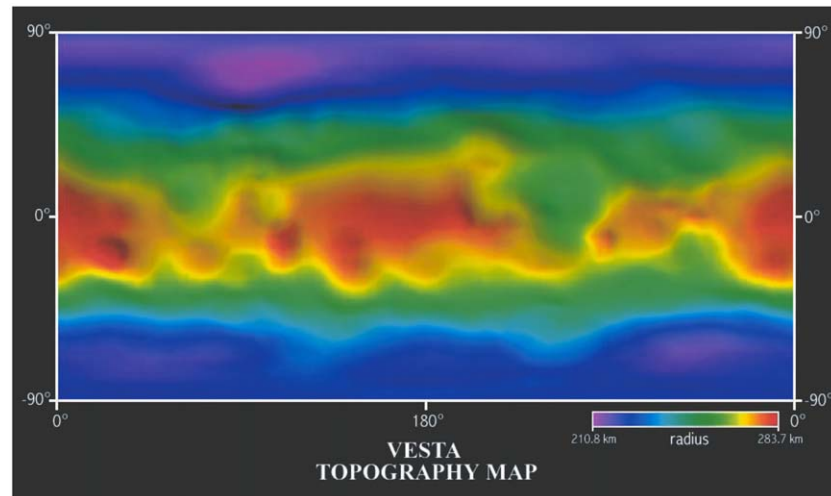
Fig. 16. Vesta topography revealed by Hubble Space Telescope imagery (Zellner and Thomas, 1997).

energies between about 0.5 and 8 MeV are measured using the ACS by isolating double interaction events. The pulse height of the first pulse of the pair provides a measure of the energy of the incident fast neutron.

4.7. Topography, geodesy and geomorphology

Planetary topography is a fundamental dataset for studies of the surfaces and interiors of solar system objects. It is required to interpret gravity data, provides a crucial third dimension to surface feature images and yields quantitative information on local surface properties such as roughness. These maps provide fundamental insight into volcanism, tectonics and cratering, and help constrain studies of the formation and evolution of the crust. Gravity studies map and model the internal density variations within the body using signals arising from the sum of the contributions from the interior density variations and surface topography. High-quality topographic information in the planetary center of mass reference frame is essential to interpret gravity data. The combination of gravity, and surface composition data is key to modeling the entire crustal composition. While the topography data for Vesta shown in Fig. 16 is the best available for any main belt asteroid, it is still far from sufficient to begin to interpret gravity data and the internal density distribution of the asteroid. The latter requires a precise determination of topography to remove its effects from the observed gravity signal. This is obtained by a mapping of surface elevations with the framing camera.

4.8. Intrinsic and induced magnetic fields

It is clear that many of the smaller objects in the solar system can generate or have generated intrinsic magnetic fields. This is true for the Earth's Moon (Russell et al., 1975), Mer-

cury (Ness et al., 1975), Ganymede (Kivelson et al., 1996). Moreover, a strongly magnetized crust has been detected at Mars (Acuña et al., 1998). The meteorites associated with Vesta, the howardites, eucrites and diogenites exhibit natural remanent magnetization that perhaps was produced in a surface magnetic field equal to or greater than that of the Earth (Collinson and Morden, 1994). The rendezvous with Vesta and Ceres by Dawn allows us to survey these objects at altitudes well below one body radius, and determine if they possess natural remanent magnetization and, through geologic correlations, when it was produced. The magnetometer also measures transient magnetic fields and how they are affected by the asteroids, providing constraints on the electrical conductivity of the interior. The response time of the Moon to step transients in the solar wind magnetic field is 80 s (Dyal and Parkin, 1973), and at Vesta should be in the range 2–8 s, easily resolvable by the 10 Hz bandwidth and 0.1 nT resolution of the magnetometer. Detection of remanent magnetization or an electrically conducting interior at Ceres would lead to a major reassessment of our present understanding of the body.

4.9. The magnetometer

These scientific objectives and our experience in the exploration of other solar system bodies enables us to develop a set of required specifications for the Dawn magnetometer. In the asteroid belt the ambient magnetic field is about 3 nT. Based on the maximum field strengths observed on the surface of the Moon on Apollo (300 nT), above the poles of Ganymede by Galileo (1000 nT) and above the crust of Mars by Mars Global Surveyor (1000 nT), we expect that the field at Vesta and Ceres at the altitude of Dawn is under 500 nT. We have conservatively chosen a ± 1000 nT range for the magnetometer, sampled at 20 Hz. The data are digitized to 16 bits providing ± 0.015 nT digitization.

Magnetic cleanliness is of concern on the Dawn mission because the magnetic field of the asteroids could be small over most of the orbit of Dawn. Dual sensors at the end of and $\frac{1}{3}$ way down the magnetometer boom provide redundancy and a measure of spacecraft magnetic fields. Since the thrusters contain strong permanent magnets and since significant currents flow from the solar array to the thrusters, we use a 5 m boom extended away from the thrusters to minimize spacecraft fields. We reverse the polarity of the magnets in one of the thrusters and rotate each about their axes of symmetry to achieve the minimum field at the sensors. This procedure with the high-order nature of the thruster field leads to an expected steady field of less than 10 nT at the sensors despite their rather high (5000 nT maximum) field at 1 m. Key components are held at fixed temperatures to eliminate temperature-dependent effects. Current levels on board are monitored and telemetered at a rate sufficient to enable the removal of the effects of varying current levels. In addition the two sensors are sampled simultaneously to provide a gradiometer measurement that verifies that the time-varying field (e.g. solar array currents) has been completely removed. Techniques used to remove unknown spacecraft and sensor-zero levels using the properties of the interplanetary magnetic field as developed for Pioneer Venus and Galileo are used to maintain the instrument baseline to better than 0.1 nT. The time-varying field is measured to 3×10^{-5} nT^2/Hz at 1 Hz. The success of the magnetics investigation depends not just on the quality of the magnetometers but also of the entire system, thus the magnetometer team leads a low-cost magnetic cleanliness program that both identifies potential magnetic problems in the design stage and verifies the success of the magnetic cleanliness program after launch.

The UCLA magnetometer (e.g. Russell et al., 1995) derives from a long line of missions including OGO5 (launched in 1968); ISEE 1 and 2 (1977), Pioneer Venus (1978), Galileo (1989), Polar (1996) and ST5 (in fabrication). The main electronics unit and a block diagram are shown in Fig. 17. The electronics unit drives the ring-core sensors shown in Fig. 18 at a frequency of 12 kHz. The amount of second harmonic signal in quadrature with the drive frequency is detected. A feedback circuit nulls the second harmonic signal by applying sufficient current to keep the ring core in zero fields. This current is a measure of the strength of the external field. The main electronics board contains a power supply, drive, sense and feedback circuitry for the three sensors together with digital conversion and command and control circuitry. The main electronics and the sensors are completely redundant, a single range and data rate and continuous operation. The only commands to the analog magnetometer are on and off. A third new technology magnetometer with a design based on the sigma delta modulator adds further redundancy. It is not needed to meet baseline requirements. This design was chosen because of its low-noise level, simplicity, low cost and its high inheritance from recent missions. The electronics unit weighs 2.35 kg,
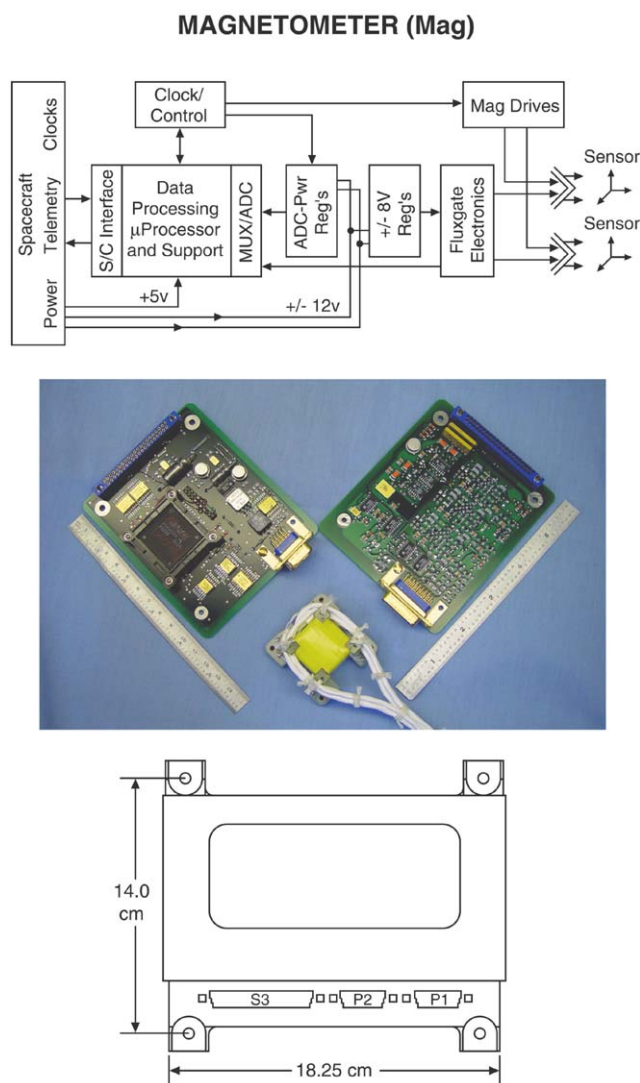

Fig. 17. Magnetometer main electronics unit block diagram (single triad) together with ST5 main electronics board.

the sensors and cable weigh 700 g, the unit draws 3.0 W of power. The magnetometer is accurately calibrated on the ground and recalibrated in flight with a precise internal calibration source.

4.10. Gravity science

The objectives of the gravity investigation are to determine the masses of the asteroids, the global gravity field of Vesta and Ceres to the 12th harmonic degree and order, the principal axes, the rotational axis, and the moments of inertia. The mass together with the shape model determines the bulk density. The shape and gravity models characterize crustal and mantle density variations Zuber et al., 2000; Zuber, 2001), and together with a detectable wobble in rotation, the possible differentiation and formation of a metallic core. Present estimates of the fractional radius of the
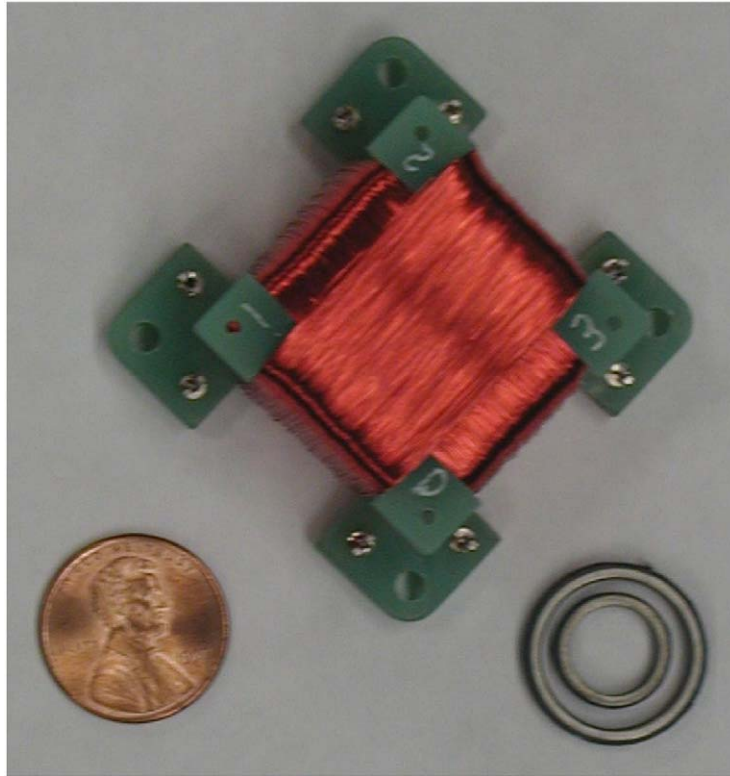
Fig. 18. Ring core sensors developed for ST5 to be used on Dawn mission.

metallic core of Vesta range up to 50%, corresponding to a fractional mass of up to 20%. If Ceres accreted water ice during formation as it presently appears, we do not expect it to be differentiated. The principal axes are determined directly from the second degree harmonics of the gravity field. The normalized polar moment of inertia (homogeneity constant) constrains the radial density distribution. Presently the densities of Ceres and Vesta are known to 2% and 3%, respectively from perturbations on other asteroids and their optically determined shapes (Hilton, 1999; Konopliv et al., 2002). The science objective is to measure the bulk density to better than 1% and Dawn will achieve relative accuracies near 0.1%.

The gravity field is determined in loose, medium and tight orbit states. In the initial "loose" orbit, only the mass is determined while optical images determine the rotational state. In the optical mapping (medium) orbit, the gravity field is determined to about degree 4. In the low altitude mapping orbit at altitudes below one body radius, the gravity field is determined up to the 12th degree. With a 12th degree gravity field, correlations with surface features on Vesta of 65 km or greater can be investigated including the large 460 km impact basin near the south pole (Thomas et al., 1997a). This higher resolution gravity field allows for comparative modeling with lunar impact basins (Zuber et al., 1994). This higher resolution gravity field is attainable since Dawn uses reaction wheels for attitude control, thus eliminating
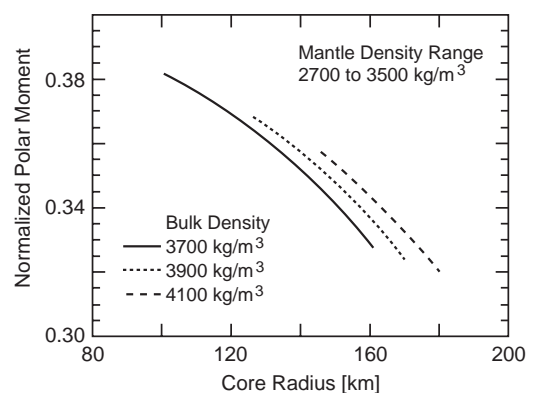

Fig. 19. Polar moment of inertia vs. core radius of Vesta.

disturbances due to thruster firings, except during orbital changes.

To use the bulk density to model the interior structure, we measure the polar moment of inertia. Fig. 19 shows the normalized polar moment of inertia, C, vs. core size for three densities and a Vesta-sized object ($C = 0.4$ implies a homogeneous body). A 1% determination of C would significantly constrain core size and composition. The detection of a wobble off the principal axes is necessary to enable C to be determined. For the NEAR mission the detection of a $0.1°$ wobble would have determined C to 1% for 433 Eros

Table 9
Data products

Instr.	Product
GR/ NS	K/Th/U maps
	O map
	Si map
	Ca map
	Al map
	Fe maps
	Mg/Ti maps
	H map
MAG	Magnetic map
FC	Global clear atlas
	Global color atlas
	Global mosaic
	Shape model
MS	Pyroxene map
	Olivine map
	Spinel map
	Geologic map
Radio Sci.	Gravity coeff. and covar.
	Free air gravity map
	Geoid and uncertainty maps
	Bouguer map

(Miller et al., 1995). We note that at Eros, no wobble was detected that was greater than 0.01° (Konopliv et al., 2002). As for NEAR, a possible Vesta and Ceres wobble will be measured by precise photogrammetric mapping and radio tracking. Whether wobble is present is determined by the recent impact history of the object.

The navigation effort is a collaboration of the radio science, and imaging teams and involves processing data from both instruments. It is closely coordinated to optimize the science return and minimize duplication of effort. The optical images for landmark observations are required for accurate navigation. Shape observations are needed for mission planning, and gravity field determination is needed for orbit determination.

5. Data analysis and archiving

The Dawn science team is committed to providing fully documented and calibrated data products of long-term use to the community, with minimal latency. During the mission, data flows from the spacecraft to UCLA, where it is validated and distributed automatically to the science teams. The raw (Level 0) data are also sent to the Planetary Data System (PDS); full documentation and software to access the data and display them is included. The science team produces and validates Level 1 calibrated data, and immediately delivers them to the PDS. The Level 2 data products described in Table 9 are released with several months of data acquisition. Existing science analysis software developed on the MGS, LP, Rosetta, NEAR and Galileo programs will be used to obtain the measurements and deductions to achieve the mission objectives. UCLA is responsible for creating an integrated mission database with science, navigation and NAIF/Spice data, accessible by the community over the web. Fully documented images will be released daily over the World Wide Web for media, educators and the public alike.

During the mission, a participating scientist (PS) program will be conducted. The objective of the PS program is to provide postdoctoral and senior scientists with opportunities for research on projects of their own choice that are compatible with the interests and goals of the Dawn mission, thus contributing to the overall science return of the mission. A list of research opportunities, each with an associated advisor/collaborator who is a member of the Dawn science team, will be offered for each competition. Proposed investigations that are unsolicited will be supervised by, or performed in collaboration with, the Dawn PI. The selected scientists will work closely with the Dawn Science Team, gaining valuable mission experience and sharing in the excitement of its discoveries. The terms of PS scientists will be for 2 years.

Data analysis by the science team begins in August, 2010, upon arrival at Vesta, and ends one year after the receipt of the last Ceres data, nominally July, 2015. A data analysis program will begin at the end of the Vesta encounter and continue until 2 years beyond the Ceres encounter. To address the range of scientific questions addressed by the large volume of diverse data to be acquired by Dawn at Vesta and Ceres we envision a data analysis program more analogous to the Mars data analysis program than the program for analysing Eros data from the NEAR mission. Most small asteroids like Eros exhibit relatively homogeneous composition and pose questions in the areas of crater mechanics and structural homogeneity (e.g., rubble pile or coherent). Vesta and Ceres similarly pose questions regarding cratering mechanics, yet they present cratering records extending over the age of the solar system (which smaller bodies do not), and heterogeneities of composition and structure over a large range of spatial scales. These protoplanets also pose questions of planetary evolution, such as differentiation, volcanism, water mobilization and transport, core formation and magnetic dynamo physics. Instruments have been chosen and data products have been designed to address these questions.

An extended mission at Ceres is possible, extending the observations there for an additional six months, to capture varying lighting conditions. If significant fuel remains after the Vesta and Ceres encounters, the spacecraft may be tasked to visit additional asteroids in a longer extended mission.

6. Education and outreach

Dawn's EPO program supports NASA's strategic plan to "Communicate widely the content, relevancy, and excitement of NASA's mission and discoveries". Furthermore, the program will involve the education community in our

endeavors to inspire and train the next generation of the nation's scientists and engineers.

Using current national standards and practices in education, the EPO team will produce content modules consisting of learning and exploration tools. These modules each cover different scientific, historical and technological aspects of the mission. The learning tools feature emerging, classroom innovations such as Calibrated Peer Review, Perceptual Learning, and others. These tools have been shown to improve student learning and comprehension. The exploration tools provide unique opportunities for students and the general public to participate in the science of the mission. For example, students will study the motion and rotational properties of Ceres and Vesta analyzing images from ground-based telescopes. The Telescopes in Education program (TIE) will be a partner in this endeavor, using an existing infrastructure of access to telescopes to study physical parameters of our targets that are important to the success of the mission.

Another exploration tool is provided by our partnership with Clickworkers. Students will study and classify craters from existing images of other planets. The nature and number of craters on Ceres and Vesta are a critical part of the scientific analysis of images returned by the Framing Camera. If students begin their studies of craters as seventh graders, they will be graduating from high school by the time the Dawn spacecraft reaches Vesta and possibly entering graduate school when we get to Ceres. The surprises gleaned from craters on Vesta and Ceres will be appreciated by those who have studied crater morphology and frequencies on other planets.

A third major exploration tool involves the Southwestern Indian Polytechnic Institute's Meteorite Identification Laboratory. Students are taught about the different types of terrestrial rocks and are encouraged to find samples of them. They are also taught the difference between terrestrial and extraterrestrial material. Although the probability of finding a meteorite is small, this program offers an opportunity for students to make scientific observations (characterize the rocks), and to understand how the instruments of the Dawn mission will search for evidence relating Vesta and Ceres to the meteorites. Making such a connection will expand our understanding of the evolution of protoplanets in the solar system.

Dawn's propulsion system is an emerging technology. We will partner with technology development efforts at JPL in bringing knowledge of ion propulsion to students and the public across the country. The history of exploration of these asteroids and the biographies of those involved in our current exploration invite students to learn and find common interests between themselves and those making the Dawn mission possible.

Dawn's EPO program was created from the following considerations:

- Products must reflect current and best education practices.
- Dissemination of materials is practical, efficient and makes good use of technology.
- Activities will leverage existing programs through partnerships established by the EPO team.

The team consists of scientists, teachers and experienced educators. A science team member leads the program with responsibility for scientific accuracy and alignment with the mission. Daily operations are managed by an experienced educator and manager. A core planning team makes detailed plans, which are implemented by a team of experienced educators from the Mid-Continent Research for Education and Learning laboratory (McREL). Materials are reviewed and tested in schools across the country. McREL's evaluation division will develop and carry out formal assessments of the materials produced by the EPO team.

Our materials and programs target key audiences including K-14 students, teachers (both in training and as professional development), the general public, and underserved and underutilized populations. We reach these audiences through activities of the OSS Solar System Exploration forum, national meetings of science, math and technology teachers and the world-wide web. Partnerships with museums and informal science centers offer another important avenue to an interested public as does the Ambassador's program sponsored by JPL. The print and television media also bring people to our web page where they can find updated information about the mission as well as access to our educational products. The EPO program will prepare the general public for the excitement of seeing these new planetary worlds and learning how they formed.

7. Concluding remarks

Dawn is clearly an ambitious mission both scientifically and technically. At the same time we believe that through maintaining simplicity and redundancy, by using proven designs and by keeping ample margins, we have produced a very robust mission. Dawn builds upon the New Millennium's Program's technological developments, transferring NASA's solar electric ion propulsion technology to the commercial sectors and putting it to work in solar system exploration. The mission has much potential to garner the public's attention, beginning just over 200 years from the discovery of Ceres and Vesta, and it can be used as a vehicle to enrich both pure and applied science curricula. Finally, the mission builds on decades of asteroid and meteoritic studies, providing the first detailed assessment of the two largest asteroids in the main belt, and setting the stage for future exploration of the main belt.

References

Acuña, M.H., et al., 1998. Magnetic field and plasma observations at Mars: initial results of the Mars Global Surveyor mission. Science 279, 1676–1680.

A'Hearn, M.F., Feldman, P.D., 1992. Water vaporization on Ceres. Icarus 98, 54–60.

Bell, J.F., 1995. EAR-A-ROR-3-52COLOR-V1.0, NASA Planetary Data System.

Bell, J.F., Davis, D.R., Gaffey, M.J., 1989. Asteroids: the big picture. In: Binzel, R.P., Gehrels, T., Matthews, M.S. (Eds.), Asteroids II. University of Arzona Press, Tucson, AZ, pp. 921–945.

Binzel, R.P., Xu, S., 1993. Chips off of asteroid 4 Vesta: evidence for the parent body of basaltic achondrite meteorites. Science 260, 186–191.

Binzel, R.P., Gaffey, M.J., Thomas, P.C., Zellner, B.H., Storrs, A.D., Wells, E.N., 1997. Geologic mapping of Vesta from 1994 Hubble Space Telescope images. Icarus 128, 95–103.

Britt, D.T., Yeomans, D., Housen, K., Consolmagno, G., 2002. Asteroid density, porosity, and structure. In: Bottke Jr., W.F., Cellino, A., Paolicchi, P., Binzel., R.P. (Eds.), Asteroids III. University of Arizona Press, Tucson, pp. 485–500.

Burbine, T.H., 1998. Could G-class asteroids be the parent bodies of the CM chondrites? Meteor. Planet. Sci. 33, 253–258.

Burbine, T.H., Buchanan, P.C., Binzel, R.P., Bus, S.J., Hiroi, T., Hinrichs, J.L., Meibom, A., McCoy, T.J., 2001. Vesta, vestoids, and the howardite, eucrite, diogenite group: relationship and the origin of spectral differences. Meteor. Planet. Sci. 36, 761–781.

Burns, R.G., 1993. Mineralogical Applications of Crystal Field Theory, Second Edition. Cambridge University Press, Cambridge, MA, p. 551.

Carlson, R.W., Lugmair, G.W., 2000. Timescales of planetesimal formation and differentiation based on extinct and extant radioisotopes. In: Canup, R.M., Righter, K. (Eds.), Origin of the Earth and Moon. University of Arizona Press, Tucson, pp. 25–44.

Clayton, R.N., Mayeda, T.K., 1996. Oxygen isotopes studies of achondrites. Geochim. Cosmochim. Acta 60, 1999–2017.

Cochran, A.L., Vilas, F., 1998. The changing spectrum of Vesta: rotationally resolved spectroscopy on surface. Icarus 134, 207–212.

Collinson, D.W., Morden, S.J., 1994. Magnetic properties of howardite, eucrite and diogenite (HED) meteorites: ancient magnetizing fields and meteorite evolution. Earth Planet. Sci. Lett. 126, 421–434.

Consolmagno, G.J., Drake, M.J., 1977. Composition and evolution of the eucrite parent body: evidence from rare earth elements. Geochim. Cosmochim. Acta 41, 1271–1282.

Coradini, A., et al., 1998. VIRTIS: an imaging spectrometer for the Rosetta mission. Planet. Space Sci. 46 (9/10), 1291–1304.

Dreibus, G., Bruckner, J., Wanke, H., 1997. On the core mass of the asteroid Vesta. Meteor. Planet. Sci. 32, A36.

Drummond, J.D., Fugate, R.Q., Christou, J.C., 1998. Full adaptive optics images of asteroids Ceres and Vesta; rotational poles and triaxial ellipsoid dimensions. Icarus 132, 80–99.

Dyal, P., Parkin, C.W., 1973. Global electromagnetic induction in the Moon and planets. Phys. Earth Planet. Inter. 7, 251–265.

Eugster, O., Michel, T., 1995. Common asteroid breakup events of eucrites, diogenites, and howardites and cosmic-ray production rates for noble gases in achondrites. Geochim. Cosmochim. Acta 59, 177–199.

Fanale, F., Salvail, J., 1989. The water regime of asteroid (1) Ceres. Icarus 82, 97–110.

Feldman, W.C., Lawrence, D.J., Elphic, R.C., Barraclough, B.L., Maurice, S., Genetay, I., Binder, A.B., 2000. Polar hydrogen deposits on the Moon. J. Geophys. Res. 105, 4175–4195.

Gaffey, M.J., 1997. Surface lithologic heterogeneity of asteroid 4 Vesta. Icarus 127, 13–157.

Gaffey, M.J., McCord, T.B., 1978. Asteroid surface materials: mineralogical characterizations from reflectance spectra. Space Sci. Rev. 21, 555–628.

Gaffey, M.J., Burbine, T.H., Binzel, R.P., 1993a. Asteroid spectroscopy: progress and perspectives. Meteoritics 28, 161–187.

Gaffey, M.J., McFadden, L.A., Nash, D., Pieters, C.M., 1993b. Ultraviolet, visible and near infra-red reflectance spectroscopy: laboratory spectra of geologic materials. In: Pieters, C.M., Englert, P.A.J. (Eds.), Remote Geochemical Analysis: Elemental and Mineralogical Composition. Cambridge University Press, New York, pp. 43–77.

Ghosh, A., McSween Jr., H.Y., 1998. A thermal model for the differentiation of asteroid 4 Vesta, based on radiogenic heating. Icarus 134, 187–206.

Gil-Hutton, R., Brunini, A., 1999. Collisional evolutional of the early asteroid belt. Planet. Space Sci. 47 (3/4), 331–338.

Grove, T.L., Bartels, K.S., 1992. The relation between diogenite cumulates and eucrite magmas. Proc. Lunar Planet. Sci. Conf. 22, 437–445.

Hewins, R.H., Newsom, H.E., 1988. Igneous activity in the early solar system. In: Kerridge, J.F., Matthews, M.S. (Eds.), Meteorites and the Early Solar System. University of Arizona Press, Tucson, pp. 73–101.

Hilton, J.L., 1999. US Naval Observatory ephemerides of the largest asteroids. Astron. J. 117, 1077–1086.

Hiroi, T., Pieters, C., Zolensky, M., Lipschutz, M., 1993. Evidence of thermal metamorphism on the C, G, B, and F asteroids. Science 261, 1016–1018.

Hiroi, T., Pieters, C.M., Takeda, H., 1994. Grain size of the surface regolith of asteroid 4 Vesta estimated from its reflectance spectrum in comparison with HED meteorites. Meteoritics 29, 394–396.

Keil, K., 2002. Geological history of asteroid 4 Vesta: the "smallest terrestrial planet". In: Bottke Jr., W.F., Cellino, A., Paolicchi, P., Binzel, R.P. (Eds.), Asteroids III. pp. 573–584.

King, T.V.V., Clark, R.N., Calvin, W.M., Sherman, D.M., Brown, R.H., 1992. Evidence for ammonium-bearing minerals on Ceres. Science 255, 1551–1553.

Kivelson, M.G., Khurana, K.K., Russell, C.T., Walker, R.J., Warnecke, J., Coroniti, F.V., Polanskey, C., Southwood, D.J., Schubert, G., 1996. Discovery of Ganymede's magnetic field by the Galileo spacecraft. Nature 384, 537–541.

Kleine, T., Munker, C., Mezger, K., Palme, H., 2002. Rapid accretion and early core formation on asteroids and the terrestrial planets from Hf-W Chronometry. Nature 418, 952–955.

Konopliv, A.S., Miller, J.K., Owen, W.M., Yeomans, D.K., Giorgini, J.D., Garmier, R., Barriot, J.P., 2002. A Global Solution for the gravity field, rotation, landmarks, and ephemeris of Eros. Icarus 160, 289–299.

Larson, H.P., Feiergerg, M.A., Fink, U., Smith, H.A., 1979. Remote spectroscopic identification of Carbonaceous chondrite mineralogies: applications to Ceres and Pallas. Icarus 39, 257–271.

Lazzaro, D., Michtchenko, T., Carvano, J.M., Binzel, R.P., Bus, S.J., Burbine, T.H., Mothe-Diniz, T., Florczak, M., Angeli, C.A., Harris, A.W., 2000. Discovery of a basaltic asteroid in the outer main belt. Science 288, 2033–2035.

Lebofsky, L.A., Feierberg, M.A., Tokunaga, A.T., Larson, H.P., Johnson, J.R., 1981. The 1.7- to 4.2-μm spectrum of asteroid 1 Ceres: evidence for structural water in clay minerals. Icarus 48, 453–459.

Longhi, J., Pan, V., 1988. Phase equilibrium constraints on the howardite-eucrite-diogenite association. Proc. Lunar Planet. Sci. Conf. 18, 459–470.

Lugmair, G.W., Shukolyukov, A., 1998. Early solar system timescales according to ^{53}Mn–^{53}Cr systematics. J. Geochim. Cosmochim. Acta 62, 2863–2886.

McCord, T.B., Sotin, C., 2003. Ceres: evolution and current state. J. Geophys. Res., submitted for publication.

McCord, T.B., Adams, J.B., Johnson, T.V., 1970. Asteroid Vesta: spectral reflectivity and compositional implications. Science 168, 1445–1447.

Michalak, G., 2000. Determination of asteroid masses I. (1) Ceres, (2) Pallas and (4) Vesta. Astron. Astrophys. 360, 363–374.

Millis, R.L., et al., 1987. The size, shape, density and albedo of Ceres from its occultation of BD + 8 deg 471. Icarus 72, 507–518.

Miller, J.K., Williams, B.G., Bollman, W.E., Davis, R.P., Helfrich, C.E., Scheeres, D.J., Synnott, S.P., Wang, T.C., Yeomans, D.K., 1995. Navigation analysis for Eros rendezvous and orbital phases. J. Astronaut. Sci. 43, 453–476.

Morden, S.J., 1992. A magnetic study of the millbillillie (eucrite) achondrite: evidence for a dynamo-type magnetising field. Meteoritics 27, 560–567.

Mitchell, D.L., Ostro, S.J., Hudson, R.S., Campbell, D.B., Velez, R., Chandler, J.F., Shapiro, I.I., Giorgini, J.D., Yeomans, D.K., 1996. Radar observations of asteroids 1 Ceres, 2 Pallas, and 4 Vesta. Icarus 124, 113–133.

Miyamoto, M., Takeda, H., 1994. Evidence for excavation of deep crustal material of a Vesta-like body from Ca compostional gradients in pyroxene. Earth Planet. Sci. Lett. 122, 343–349.

Ness, N.F., Behannon, K.W., Lepping, R.P., Wheng, Y.C., 1975. The magnetic field of Mercury I. J. Geophys. Res. 80, 2708–2716.

Nyquist, L.E., Bogard, D., Takeda, H., Bansal, B., Wiesmann, H., Shih, C.Y., 1997. Crystallization, recrystallization, and impact-metamorphic ages of eucrites Y792510 and Y791186. Geochim. Cosmochim. Acta 61, 2119–2138.

Papike, J.J., 1998. Comparative planetary mineralogy: chemistry of melt-derived pyroxene, feldspar, and olivine. In: Papike, J.J. (Ed.), Planetary Materials. pp. 7–1 to 7–11. Rev. Mineral. 36, Min. Soc. Amer., Washington.

Parker, J.W., Stern, S.A., Thomas, P.C., Festou, M.C., Merline, W.J., Young, E.F., Binzel, R.P., Lebofsky, L.A., 2002. Analysis of the first disk-resolved images of Ceres from ultraviolet observations with the Hubble Space Telescope. Astron. J. 123, 549–557.

Pieters, C.M., McFadden, L.A., 1994. Meteorite and asteroid reflectance spectroscopy: clues to early solar system processes. Annu. Rev. Earth Planet. Sci. 22, 457–497.

Pieters, C.M., Mustard, J.F., Sunshine, J.M., 1996. Quantitative mineral analyses of planetary surfaces using reflectance spectroscopy. In: Dyar, M.D., McCammon, Schafer, M. (Eds.), Mineral Spectroscopy: A Tribute to R. G. Burns. The Geochemistry Society, University Park, PA, pp. 307–325.

Prettyman, T.H., Feldman, W.C., Fuller, K.R., Storms, S.A., Soldner, S.A., Szeles, Cs., Ameduri, F.P., Lawrence, D.J., Browne, M.C., Moss, C.E., 2002. CdZnTe gamma-ray spectrometer for orbital planetary missions. IEEE Trans. Nucl. Sci. 49, 1881–1886.

Prettyman, T.H., Feldman, W.C., Ameduri, F.P., Barraclough, B.L., Cascio, E.W., Fuller, K.R., Funsten, H.O., Lawrence, D.J., McKinney, G.W., Russell, C.T., Soldner, S.A., Storms, S.A., Szeles, Cs., Tokar, R.L., 2003. Gamma ray and neutron spectrometer for the dawn mission to 1 Ceres and 4 Vesta. IEEE Trans. Nucl. Sci. 50, 1190–1197.

Reininger, F., et al., 1996. VIRTIS: visible infrared thermal imaging spectrometer for the Rosetta Mission. SPIE 2819, 66–77.

Righter, K., Drake, M.J., 1996. Core formation in the Earth's Moon, Mars and Vesta. Icarus 124, 513–529.

Righter, K., Drake, M.J., 1997. A magma ocean on Vesta: core formation and petrogenesis of eucrites and diogenites. Meteor. Planet. Sci. 32, 929–944.

Rivkin, A.S., 1997. Observations of main-belt asteroids in the 3-micron region. Ph.D. Thesis, University of Arizona.

Russell, C.T., Coleman Jr., P.J., Fleming, B.K., Hilburn, L., Ioannidis, G., Lichtenstein, B.R., Schubert, G., 1975. The fine scale lunar magnetic field. Proc. Lunar Sci. Conf. 6, 2955–2969.

Russell, C.T., Snare, R.C., Means, J.D., Pierce, D., Dearborn, D., Larson, M., Barr, G., Le, G., 1995. The GGS/polar magnetic fields investigation. Space Sci. Rev. 71 (1–4), 563–582.

Ruzicka, A., Snyder, G.A., Taylor, L.A., 1997. Vesta as the howardite, eucrite and diogenite parent body: implications for the size of a core and for large-scale differentiation. Meteor. Planet. Sci. 32, 825–840.

Saint-Pe, O., Combes, M., Rigaut, F., 1993. Ceres surface properties by high-resolution imaging from Earth. Icarus 105, 271–281.

Sato, K., Miyamoto, M., Zolensky, M.E., 1997. Absorption bands near three micronmeters in diffuse reflectance spectra of carbonaceous chondrites: comparison with asteroids. Meteor. Planet. Sci. 32, 503–507.

Schubart, J., Matson, D.L., 1979. Masses and densities of asteroids. In: Gehrels, T. (Ed.), Asteroids. University of Arizona Press, Tucson, pp. 84–97.

Standish, E.M., Hellings, R.W., 1989. A determination of the masses of Ceres, Pallas, and Vesta from their perturbations upon the orbit of Mars. Icarus 80, 326–333.

Srinivasan, G., Goswami, J.N., Bhandari, N., 1999. ^{26}Al in eucrite Piplia Kalan: plausible heat source and formation chronology. Science 284, 1348–1350.

Stolper, E., 1977. Experimental petrology of eucrite meteorites. Geochim. Cosmochim. Acta 41, 587–611.

Taylor, S.R., 1992. Solar System Evolution, A New Perspective. Cambridge University Press, Cambridge, MA, p. 75.

Tedesco, E.F., Williams, J.G., Matson, D.L., Veeder, G.J., Gradie, J.G., Lebotsky, L.A., 1989. A three parameter asteroid taxonomy. Astron. J. 97, 580–606.

Tera, F., Carlson, R.W., Boctor, N.Z., 1997. Contrasting Pb–Pb ages of basaltic achondrites and their relation to the early history of the solar system. Geochim. Cosmochim. Acta 61, 1713–1732.

Thomas, P.C., Binzel, R.P., Gaffey, M.J., Storrs, A.D., Wells, E.N., Zellner, B.H., 1997a. Impact excavation on asteroid 4 Vesta: Hubble Space Telescope results. Science 277, 1492–1495.

Thomas, P.C., Binzel, R.P., Gaffey, M.J., Zellner, B.H., Storrs, A.D., Wells, E.N., 1997b. Vesta: spin pole, size and shape from HST images. Icarus 128, 88–94.

Viateau, B., Rapaport, M., 1998. The mass of (1) Ceres from its gravitational perturbations on the orbits of 9 asteroids. Astron. Astrophys. 334, 729–735.

Vilas, F., 1994. A cheaper, faster, better way to detect water of hydration on solar system bodies. Icarus 111, 456–467.

Vilas, F., Gaffey, M.J., 1989. Phyllosilicate absorption features in main-belt and outer-belt asteroid reflectance spectra. Science 246, 790–792.

Vilas, F., Cochran, A.L., Jarvis, K.S., 2000. Vesta and the vestoids: a new rock group?. Icarus 147, 119–128.

Warren, P.H., 1997. Magnesium oxide–iron oxide mass balance constraints and a more detailed model for the relationship between eucrites and diogenites. Meteor. Planet. Sci. 32, 945–963.

Webster, W.J., Johnston, K.J., 1989. Passive microwave observations of asteroids. In: Binzel, R.P., Gehrels, T., Matthews, M.S. (Eds.), Asteroids II. University of Arizona Press, Tucson, pp. 213–227.

Welten, K.C., Lindner, L., Van der Borg, K., Loeken, T., Scherer, P., Schultz, L., 1997. Cosmic-ray exposure ages of diogenites and the recent collisional history of the howardite, eucrite and diogenite parent body/bodies. Meteor. Planet. Sci. 32, 891–902.

Wilson, L., Keil, K., 1996. Volcanic eruptions and intrusions on the asteroid 4 Vesta. J. Geophys. Res. 101, 18,927–18,940.

Wisdom, J., 1985. Meteorites may follow a chaotic path to Earth. Nature 315, 731–733.

Yamada, M., Sasaki, S., Nagahara, H., Fuiwara, A., Hasegawa, S., Yano, H., Hiroi, T., Obashi, H., Ohtake, H., 1999. Simulation of space weathering of planet-forming materials: nano-second pulse laser irradiation and proton implantation on olivine and pyroxene samples. Earth Planets Space 51, 1255–1265.

Yamaguchi, A., Taylor, G.J., Keil, K., 1996. Global crustal metamorphism of the eucrite parent body. Icarus 124, 97–112.

Yamaguchi, A., Taylor, G.J., Keil, K., 1997. Metamorphic history of the eucritic crust of 4 Vesta. J. Geophys. Res. 102, 13,381–13,386.

Yin, Q., Jacobsen, S.B., Yamashita, K., Blichart-Trott, J., Telouk, P., Albarede, F., 2002. A short timescale for terrestrial planet formation from Hf-W Chronometry of meteorites. Nature 418, 949–952.

Zellner, B.H., Thomas, P.C., 1997. Space Telescope Science Institute Press Release 1997-27.

Zuber, M.T., 2001. The crust and mantle of Mars. Nature 412, 220–227.

Zuber, M.T., Smith, D.E., Lemoine, F.G., Neumann, G.A., 1994. The shape and internal structure of the moon from the Clementine Mission. Science 266, 1839–1843.

Zuber, M.T., Solomon, S.C., Phillips, R.J., Smith, D.E., Tyler, G.L., Aharonson, O., Balmino, G., Banerdt, W.B., Head, J.W., Lemoine, F.G., McGovern, P.J., Neumann, G.A., Rowlands, D.D., 2000. Internal structure and early thermal evolution of Mars from Mars Global Surveyor topography and gravity. Science 287, 1788–1793.